

Population oscillations in spatial stochastic Lotka–Volterra models: A field-theoretic perturbational analysis

Uwe C. Täuber

Department of Physics, Virginia Tech, Blacksburg, VA 24061-0435, USA

E-mail: tauber@vt.edu

Abstract. Field theory tools are applied to analytically study fluctuation and correlation effects in spatially extended stochastic predator-prey systems. In the mean-field rate equation approximation, the classic Lotka–Volterra model is characterized by neutral cycles in phase space, describing undamped oscillations for both predator and prey populations. In contrast, Monte Carlo simulations for stochastic two-species predator-prey reaction systems on regular lattices display complex spatio-temporal structures associated with persistent erratic population oscillations. The Doi–Peliti path integral representation of the master equation for stochastic particle interaction models is utilized to arrive at a field theory action for spatial Lotka–Volterra models in the continuum limit. In the species coexistence phase, a perturbation expansion with respect to the nonlinear predation rate is employed to demonstrate that spatial degrees of freedom and stochastic noise induce instabilities toward structure formation, and to compute the fluctuation corrections for the oscillation frequency and diffusion coefficient. The drastic downward renormalization of the frequency and the enhanced diffusivity are in excellent qualitative agreement with Monte Carlo simulation data.

PACS numbers: 87.23.Cc, 02.50.Ey, 05.40.-a, 87.18.Tt

Submitted to: *J. Phys. A: Math. Gen.* — 27 January 2023

1. Introduction

In the past two decades or so, analytical and computational tools developed in statistical physics have been quite successfully applied to mathematical problems in ecology and population dynamics, with the overall goal to arrive at a quantitative understanding of the emergence of biodiversity in nature [1]–[4]. The typical physics approach to complex dynamical systems is of course to first consider perhaps oversimplified idealized models that however are designed to hopefully capture the essential phenomenology. Whereas a considerable part of the mathematical biology literature largely addresses coupled deterministic equations of motion for interacting population species that are ultimately based on mean-field type rate equation approximations, leaving aside some of

the biological complexity provides the opportunity to consistently incorporate stochastic fluctuations and spatio-temporal correlations, whose crucial importance has long been recognized in the field [5].

This paper addresses predator-prey competition models that are defined via reaction-diffusion systems on a regular d -dimensional lattice, and whose rate equations in the well-mixed mean-field limit reduce to the two coupled ordinary differential equations originally introduced independently by Lotka [6] and Volterra [7] nearly a century ago. These stochastic spatial predator-prey models have served as paradigmatic examples for the emergence of cooperative steady states in the dynamics of two competing populations [8]–[10] (see also Ref. [11] for a fairly recent overview). The deterministic Lotka–Volterra rate equation model is characterized by a neutral cycle in phase space, describing regular undamped nonlinear population oscillations with the unrealistic feature that both predator and prey population densities invariably return to their initial values. In contrast, computer simulations of sufficiently large stochastic Lotka–Volterra systems yield long-lived erratic population oscillations [12]–[19], whose persistence can be understood through a resonant stochastic amplification mechanism [20] that drastically extends the transient time interval before any finite system ultimately reaches its absorbing stationary state, where the predator population becomes extinct [21, 22]. In spatially extended systems, already the mean-field Lotka–Volterra reaction-diffusion equations allow for traveling wave solutions [23]–[25]. In the corresponding stochastic lattice realizations, these regular wave crests become spreading activity fronts [26] that further enhance both populations’ life span, and furthermore induce short-ranged but significant positive correlations between representatives of either species, and anti-correlations between the predator and prey populations [11, 27]. Over the past years, we have investigated various different variants of such two-species stochastic spatial Lotka–Volterra models for competing predator-prey populations, and found these intriguing spatio-temporal structures to be remarkably stable with respect to modifications of the detailed microscopic interaction rules [27, 28]. Even in the presence of quenched spatial disorder in the reaction rates, the qualitative features of spatial stochastic Lotka–Volterra models remain unchanged, although quite remarkably both the predator and prey populations benefit from such environmental variability [29].

Many qualitative features of stochastic spatial predator-prey systems are adequately captured by the associated coupled mean-field rate equations, augmented with diffusive spreading. However, one observes strikingly strong quantitative renormalizations of, e.g., the characteristic population oscillation frequency, whose numerically determined values in various systems were found to be reduced as compared with the (linearized) rate equation predictions by factors in the range $2 \dots 6$, depending on the reaction rates, both in the presence and absence of site occupation number restrictions for the predator and prey populations [11, 27]. In addition, the neutral cycle oscillations in the original Lotka–Volterra rate equations are undamped; in contrast, when a finite carrying capacity for the prey species is imposed, the system relaxes to a stable coexistence fixed point. However, starting from random initial states, Monte Carlo simulations for the corresponding

stochastic lattice models yield initially damped population oscillations in the coexistence phase, even in the absence of any restrictions on the site occupation numbers, i.e., for infinite local carrying capacities. These are associated with striking spatio-temporal structures, namely spreading waves of prey closely followed by predators. In our Monte Carlo simulations, we measured the front speed to be markedly enhanced with respect to the mean-field prediction [29].

The aim of this present paper is to provide a qualitative and even semi-quantitative explanation for these intriguing observations. The Doi–Peliti coherent-state path integral representation of the master equation for stochastic interacting particle systems [30]–[33] (for recent reviews, see Refs. [34, 35]), augmented with a means to incorporate restricted site occupation numbers [36], will be employed to gain a comprehensive understanding of fluctuation and correlation effects in stochastic spatial predator-prey models. More specifically, a perturbative loop expansion to first order in the nonlinear predation rate will be constructed; it will allow us to demonstrate the instability of the spatial stochastic system against dynamic structure formation, and enable the computation of the fluctuation-induced renormalizations of the population oscillation frequency and diffusion coefficient [37].

This very same formalism was already utilized in Ref. [11] to demonstrate with the aid of renormalization group arguments that the effective critical field theory in the vicinity of the predator extinction threshold that emerges at low predation rate for finite prey carrying capacity can be mapped onto Reggeon field theory which encapsulates the universal scaling behavior of critical directed percolation clusters [38]–[41]. Indeed, since the predator extinction transition represents a continuous nonequilibrium phase transition from an active stationary to an inactive, absorbing state (in the absence of any conserved quantities and quenched disorder), one would expect it to be governed by the prominent directed percolation universality class [40]–[45]. There exists now ample numerical evidence that the critical exponent values at or near the predator extinction transition in spatially extended Lotka–Volterra systems are in fact those of directed percolation [9]–[19]. The present work also complements and transcends the treatment in Ref. [46] where the same mathematical framework was utilized as a starting point for a van-Kampen system size expansion, demonstrating the persistence of population oscillations in the species coexistence phase of stochastic lattice Lotka–Volterra models, thus generalizing the zero-dimensional analysis in Ref. [20] to spatially extended systems.

This paper is structured as follows: The following section begins with a concise review of the properties of the Lotka–Volterra mean-field rate equations, including the modifications induced by a finite prey carrying capacity, and some crucial features observed in Monte Carlo simulations for stochastic two-species predator-prey models on a regular lattice. Next the construction of the Doi–Peliti path integral representation is explained, and its utility demonstrated by a brief summary of the crucial steps that allow a mapping of the Lotka–Volterra system with finite local prey carrying capacity near the predator extinction threshold onto Reggeon field theory that governs the directed percolation universality class. Subsequently, this formalism is employed to construct

a systematic perturbation expansion with respect to the nonlinear predation rate in the species coexistence phase. We then establish the presence of structure formation instabilities, and proceed to compute the renormalized population oscillation frequency and diffusivity to one-loop order, and compare our results with simulation data. The conclusion summarizes these novel results, and gives an outlook to future investigations. Two appendices provide additional technical details and an integral table.

2. Stochastic lattice Lotka–Volterra models

We begin by first defining the stochastic interacting particle model under consideration through a set of coupled irreversible ‘chemical’ reactions, and then provide a summary of its basic features as obtained in the mean-field rate equation approximation. Next we discuss the crucial numerical observations from the extensive literature for stochastic spatially extended two-species predator-prey systems.

2.1. Model variants and mean-field description

We consider a system comprised of two distinct particle species that propagate diffusively with continuum diffusion constants $D_{A/B}$ and undergo the following stochastic reactions:



The ‘predators’ A decay or die spontaneously at rate $\mu > 0$, whereas the ‘prey’ B produce offspring with rate $\sigma > 0$. In the absence of the binary ‘predation’ interaction with rate λ , the uncoupled first-order processes would naturally lead to predator extinction $a(t) = a(0) e^{-\mu t}$, and Malthusian prey population explosion $b(t) = b(0) e^{\sigma t}$; here $a(t)$ and $b(t)$ respectively indicate the $A(B)$ concentrations or population densities. The predation reaction constitutes a nonlinear interaction that simultaneously controls the prey particle number and allows the predators to multiply, thus opening the possibility of species coexistence through competition.

In the simplest spatial realization of this stochastic reaction-diffusion model, both particle species are represented by unbiased random walkers on a d -dimensional hypercubic lattice (with lattice constant a_0), and one allows an arbitrary number of particles per lattice site (see Ref. [27]). The reactions (1) can then all be implemented strictly on-site: Offspring particles are placed on the same lattice point as their parents, and the predation reaction happens only if an A and a B particle meet on the same lattice site. If one further assumes the populations to remain well mixed, and consequently ignores both spatial fluctuations and correlations, the coupled reactions (1) can approximately be described through the associated mean-field rate equations for spatially homogeneous concentrations $a(t) = \langle a(\vec{x}, t) \rangle$, $b(t) = \langle b(\vec{x}, t) \rangle$, where $a(\vec{x}, t)$ and $b(\vec{x}, t)$ respectively denote the local predator and prey densities. With $\lambda = a_0^d \lambda'$,

this leads to the two classical Lotka–Volterra coupled ordinary nonlinear differential equations [4]:

$$\dot{a}(t) = \lambda a(t) b(t) - \mu a(t) , \quad \dot{b}(t) = \sigma b(t) - \lambda a(t) b(t) . \quad (2)$$

The rate equations (2) display three stationary states (a_s, b_s) : (i) the empty absorbing state (total population extinction) $(0, 0)$, which is obviously linearly unstable if $\sigma > 0$; (ii) an absorbing state wherein the predators go extinct and the prey population diverges $(0, \infty)$, which for $\lambda > 0$ is also linearly unstable; and (iii) a species coexistence state $(a_u = \sigma/\lambda, b_u = \mu/\lambda)$, which represents a marginally stable fixed point with purely imaginary eigenvalues $\pm i\omega_0$ of the associated Jacobian stability matrix, with the (linear) oscillation frequency $\omega_0 = 2\pi f_0 = \sqrt{\mu\sigma}$ about the center fixed point (a_u, b_u) . In the full nonlinear ordinary differential equation system (2), the phase space trajectories are determined by $da/db = [a(\lambda b - \mu)]/[b(\sigma - \lambda a)]$, for which one easily identifies the conserved first integral $K(t) = \lambda[a(t) + b(t)] - \sigma \ln a(t) - \mu \ln b(t) = K(0)$. As a consequence, the solutions of the deterministic Lotka–Volterra rate equations form closed orbits in phase space that describe regular periodic nonlinear population oscillations whose amplitudes and phases are fixed by the initial configuration. Naturally, the neutral cycles of the coupled mean-field rate equations (2) that appear independent of the set rates and take the system precisely back to its initial configuration after one period represent biologically unrealistic features, and are moreover indicative of the fundamental instability of this deterministic mathematical model with respect to even slight modifications [4].

One important example of such an alteration that aims at rendering the Lotka–Volterra system more relevant to ecology is to introduce a finite carrying capacity (maximum total particle density) $\rho > 0$ that limits the prey population growth [4]. It can be interpreted as originating from, e.g., limited food resources for the prey species. Within the mean-field rate equation framework, the second differential equation in (2) then becomes replaced with

$$\dot{b}(t) = \sigma b(t) [1 - b(t)/\rho] - \lambda a(t) b(t) . \quad (3)$$

Again, one finds three stationary states in this restricted Lotka–Volterra model: (i) total extinction $(0, 0)$; (ii') predator extinction and prey saturation $(0, \rho)$, which becomes linearly stable for sufficiently small predation rates $\lambda < \lambda_c = \mu/\rho$; (iii') species coexistence (a_r, b_r) with $a_r = (1 - \mu/\rho\lambda) \sigma/\lambda$ and $b_r = \mu/\lambda$, which comes into existence and is linearly stable if the predation rate exceeds the threshold λ_c . The finite carrying capacity causes the Jacobian matrix eigenvalues to acquire negative real parts, indicating an exponential approach to the stable fixed point (a_r, b_r) :

$$\epsilon_{\pm} = -\frac{\mu\sigma}{2\rho\lambda} \left[1 \pm \sqrt{1 - \frac{4\rho\lambda}{\sigma} \left(\frac{\rho\lambda}{\mu} - 1 \right)} \right] . \quad (4)$$

The neutral cycles of the unrestricted model (2) are thus replaced either by a stable node for which ϵ_{\pm} are both real, namely when $\sigma > \sigma_s = 4\lambda\rho(\rho\lambda/\mu - 1) > 0$, or alternatively $\mu/\rho < \lambda < \lambda_s = (1 + \sqrt{1 + \sigma/\mu}) \mu/2\rho$; or by a stable focus with complex

conjugate stability matrix eigenvalue pair, and consequent spiraling relaxation towards the fixed point if $\sigma < \sigma_s$ or $\lambda > \lambda_s$. In this situation, both predator and prey populations approach their stationary values (a_r, b_r) via damped oscillations. Adding spatial degrees of freedom, finite local carrying capacities can be implemented in a lattice model through limiting the maximum occupation number per site for each species. Most drastically, one can permit at most a single particle per lattice site (as, for example, implemented in Ref. [11]); the binary predation reaction then has to occur between predators and prey on nearest-neighbor sites, and new offspring is to be placed on adjacent positions. In that case, one may actually dispense with hopping processes, since all particle production reactions automatically entail population spreading. Upon adding diffusive spreading terms (with diffusivities D_A, D_B) to the mean-field rate equations, one may describe spreading activity fronts of prey invading empty regions followed by predators feeding on them. A well-established lower bound for the front propagation speed is [23, 24, 4]

$$v_{\text{front}} > \sqrt{4 D_A (\lambda \rho - \mu)} . \quad (5)$$

To summarize, within the mean-field rate approximation, a finite prey carrying capacity ρ , which can be viewed as the mean result of local restrictions on the prey density originating from limited resources, crucially changes the phase diagram: There emerges an extinction threshold (at λ_c for fixed μ) for the predator population, which in a spatially extended system in the thermodynamic and infinite-time limit becomes a genuine continuous nonequilibrium phase transition from an active to an absorbing state. In addition, deep in the species coexistence phase the restricted Lotka–Volterra model is characterized by transient decaying population oscillations, which become overdamped upon approaching the predator extinction threshold.

2.2. Monte Carlo simulation results in the species coexistence phase

Various authors have studied individual-based stochastic lattice predator-prey models, predominantly in two dimensions and typically with periodic boundary conditions, that in the well-mixed mean-field limit reduce to the classical Lotka–Volterra system; see Refs. [8]–[19] and [27] for a partial listing. The following is a concise summary of some fundamental results from these extensive numerical investigations, as pertinent for the subsequent field-theoretic analysis.

Monte Carlo simulations in two dimensions, both in the absence and presence of local density limitations, observe the emergence of prominent spatio-temporal structures associated with remarkably strong fluctuations in the species coexistence phase, even far away from the continuous nonequilibrium predator extinction transition. Spherically expanding growth fronts of prey closely followed by predators periodically sweep the system; any small surviving clusters of prey then serve as nucleation centers for new population waves that subsequently interact and for large population densities eventually merge with each other. These spreading activity fronts are especially sharp for the site-restricted model variants, whereas in simulation runs performed with arbitrarily many particles per site, the fronts appear more diffuse and localized [26]. Equal-time

density correlation functions can be employed to determine the spatial width $\sim 10 \dots 20$ lattice sites of the spreading activity regions [11, 27, 29]. In comparison with the mean-field bound (5), the front velocity was measured to be typically enhanced by a factor up to $\sim 2 \dots 3$ in simulation runs starting with a single localized activity seed [29].

Averaging over the weakly coupled and periodically emerging structures yields long-lived but damped population oscillations. As the system size increases, one observes the relative oscillation amplitudes to decrease; in the thermodynamic limit, the quasi-periodic population fluctuations eventually terminate. Yet locally density oscillations persist for both predators and prey species. In the absence of spatial degrees of freedom, these can be understood by performing a van-Kampen system size expansion about the absorbing steady state [20]. The fluctuation corrections may then essentially be described by means of a damped harmonic oscillator driven by white noise that will on occasion resonantly incite large-amplitude excursions away from the stable fixed point in the phase plane.

From the prominent peaks detected in the Fourier-transformed concentration signals, characteristic oscillation frequencies can be inferred [11, 27, 29]. The thus numerically determined typical population oscillation frequencies are found to be reduced by a factor ranging between 2 and 6 (depending on the other rates) in the stochastic spatially extended system as compared to the mean-field prediction, a considerable downward renormalization obviously caused by fluctuations and reaction-induced spatio-temporal correlations; compare Fig. 9 in Ref. [11] and Fig. 6(b) in Ref. [27]. However, the measured oscillation frequencies f roughly follow the square-root dependence on the rates μ and σ suggested by the linearized mean-field approximation: $\omega_0 = 2\pi f_0 = \sqrt{\mu\sigma}$, yet with noticeable deviations once either σ or μ significantly differ from unity. In addition, the functional dependence of f on the rates μ and σ is surprisingly similar, at least in a mid-range interval of values for both rates near 1. As we shall see in section 4, these observations and quantitative trends are remarkably accurately reproduced by a first-order analytic perturbation theory for fluctuation corrections in stochastic lattice Lotka–Volterra models.

As the predation efficiency λ is reduced (with all other parameters held constant), stochastic lattice Lotka–Volterra systems with site occupation restrictions display just the same qualitative scenarios as revealed by the mean-field analysis for eqs. (3) with finite prey carrying capacity: First, the focal stationary points in the phase plane are replaced by stable nodes (corresponding to real stability matrix eigenvalues); the population oscillations then cease, and no interesting spatial structures are discernible aside from hardly fluctuating localized clusters of predators in a ‘sea’ of prey that almost fill the entire lattice [26]. At a sufficiently small critical value λ_c , at last the predator extinction threshold is encountered, and the measured critical scaling laws near this active- to absorbing state transition are very well described by the accepted critical exponents of directed percolation [9]–[19].

Simulations in one dimension (usually on a circular domain) yield a crucial difference between model variants that incorporate or neglect site occupation number

restrictions: In the former situation, the A and B particles quickly segregate into distinct domains, with the predation reactions occurring only at their boundaries. The long-time evolution is consequently dictated by the very slow coarsening of merging predator domains [11]. In contrast, in the absence of site occupation restrictions, one observes the system to invariably remain in an active fluctuating coexistence state [27].

We finally remark that the above statements naturally all pertain to sufficiently large lattices. Of course, any finite system with an absorbing steady state will in principle eventually reach and remain trapped in it. However, the associated typical extinction times are understood to grow fast with system size, namely according to a power law [21, 22]; simulation runs performed in reasonably large lattices consequently never reach this extinction state during their entire duration.

3. Field-theoretic analysis

This section will first provide a brief overview how a coherent-state path integral representation can be constructed directly from the fundamental master equation that defines a stochastic interacting particle system [30]–[35], see also Refs. [47, 48]. This field-theoretic representation faithfully encodes statistical fluctuations, including those caused by discreteness and the internal reaction noise, as well as emerging correlations in spatial reaction-diffusion systems, and allows for systematic approximative analysis, as will be detailed below for two-species predator-prey models. For the sake of completeness, the essential steps of mapping spatial stochastic Lotka–Volterra models with site occupation number restrictions near the predator extinction threshold onto Reggeon field theory [11] will be repeated here as well. The subsequent section 4 is then concerned with fluctuation corrections in the two-species coexistence phase, which become manifest through propagator renormalizations.

3.1. Field theory representation

The Doi–Peliti approach is based on the fact that at any time the configurations in locally reacting particle systems can be enumerated through specifying the occupation numbers of each species per lattice site i , say here n_i for the predators A and m_i for the prey B , and that the effect of any allowed stochastic process is to merely modify these on-site integer occupation numbers. For now, arbitrarily many particles of either species are allowed to occupy any lattice point: $n_i, m_i = 0, 1, \dots, \infty$. The master equation for our local reaction scheme (1) that governs the time evolution of the configurational probability to find n_i predators and m_i prey on site i at time t through the balance of gain and loss terms reads

$$\begin{aligned} \frac{\partial}{\partial t} P(n_i, m_i; t) = & \mu \left[(n_i + 1) P(n_i + 1, m_i; t) - n_i P(n_i, m_i; t) \right] \\ & + \sigma \left[(m_i - 1) P(n_i, m_i - 1; t) - m_i P(n_i, m_i; t) \right] \\ & + \lambda' \left[(n_i - 1) (m_i + 1) P(n_i - 1, m_i + 1; t) - n_i m_i P(n_i, m_i; t) \right]. \end{aligned} \quad (6)$$

As initial condition, we may for instance choose a Poisson distribution $P(n_i, m_i; 0) = \bar{n}_0^{n_i} \bar{m}_0^{m_i} e^{-\bar{n}_0 - \bar{m}_0} / n_i! m_i!$ with mean initial predator and prey concentrations \bar{n}_0 and \bar{m}_0 .

Because all reactions just change the site occupation numbers by integer values, a Fock space representation is particularly useful. To this end, we introduce the bosonic ladder operator algebra $[a_i, a_j] = 0$, $[a_i, a_j^\dagger] = \delta_{ij}$ for species A , from which we construct the predator particle number eigenstates $|n_i\rangle$, $a_i |n_i\rangle = n_i |n_i - 1\rangle$, $a_i^\dagger |n_i\rangle = |n_i + 1\rangle$, $a_i^\dagger a_i |n_i\rangle = n_i |n_i\rangle$. A Fock state with n_i particles on site i is obtained from the empty ‘vacuum’ configuration $|0\rangle$, defined via $a_i |0\rangle = 0$, through $|n_i\rangle = a_i^{\dagger n_i} |0\rangle$. In the same manner, we proceed for the prey particles, with associated annihilation and creation operators b_i and b_i^\dagger that all commute with the predator ladder operators: $[a_i, b_j] = 0 = [a_i, b_j^\dagger]$.

To implement the stochastic kinetics for the entire lattice, one considers the master equation for the configurational probability $P(\{n_i\}, \{m_i\}; t)$, given by a sum over all lattice points of the right-hand-side of eq. (6), and recognizes that a general Fock state is constructed by the tensor product $|\{n_i\}, \{m_i\}\rangle = \prod_i |n_i\rangle |m_i\rangle$. One then defines a time-dependent formal state vector through a linear combination of all possible Fock states, weighted by their configurational probability at time t :

$$|\Phi(t)\rangle = \sum_{\{n_i\}, \{m_i\}} P(\{n_i\}, \{m_i\}; t) |\{n_i\}, \{m_i\}\rangle . \quad (7)$$

This superposition state thus encodes the stochastic temporal evolution. Straightforward manipulations now transform the time dependence from the linear master equation into an ‘imaginary-time’ Schrödinger equation, governed by a time-independent stochastic Liouville time evolution operator H :

$$\frac{\partial |\Phi(t)\rangle}{\partial t} = -H |\Phi(t)\rangle , \quad \text{or} \quad |\Phi(t)\rangle = e^{-Ht} |\Phi(0)\rangle . \quad (8)$$

For on-site reactions, $H_{\text{reac}} = \sum_i H_r(a_i^\dagger, b_i^\dagger; a_i, b_i)$ is a sum of local (normal-ordered) contributions; for the Lotka–Volterra predator-prey system one obtains

$$H_{\text{reac}} = - \sum_i \left[\mu (1 - a_i^\dagger) a_i + \sigma (b_i^\dagger - 1) b_i^\dagger b_i + \lambda' (a_i^\dagger - b_i^\dagger) a_i^\dagger a_i b_i \right] . \quad (9)$$

Note that each reaction process is represented by two contributions, originating respectively from the gain and loss terms in the master equation. For nearest-neighbor hopping of particles $A(B)$ with rate $D'_A(h_B)$ between neighboring lattice sites $\langle ij \rangle$, one finds the additional contributions

$$H_{\text{diff}} = \sum_{\langle ij \rangle} \left[D'_A (a_i^\dagger - a_j^\dagger) (a_i - a_j) + D'_B (b_i^\dagger - b_j^\dagger) (b_i - b_j) \right] . \quad (10)$$

Our goal is to compute averages and correlation functions with respect to the configurational probability $P(\{n_i\}, \{m_i\}; t)$ which is accomplished by means of the projection state $\langle \mathcal{P} | = \langle 0 | \prod_i e^{a_i} e^{b_i}$, for which $\langle \mathcal{P} | 0 \rangle = 1$ and $\langle \mathcal{P} | a_i^\dagger = \langle \mathcal{P} | = \langle \mathcal{P} | b_i^\dagger$, since $[e^{a_i}, a_j^\dagger] = e^{a_i} \delta_{ij}$. For the desired statistical averages of observables \mathcal{O} , which

naturally must all be expressible as functions of the occupation numbers n_i and m_i , one obtains

$$\langle \mathcal{O}(t) \rangle = \sum_{\{n_i\}, \{m_i\}} \mathcal{O}(\{n_i\}, \{m_i\}) P(\{n_i\}, \{m_i\}; t) = \langle \mathcal{P} | \mathcal{O}(\{a_i^\dagger a_i\}, \{b_i^\dagger b_i\}) | \Phi(t) \rangle. \quad (11)$$

As a consequence of probability conservation, one finds for $\mathcal{O} = 1$: $1 = \langle \mathcal{P} | \Phi(t) \rangle = \langle \mathcal{P} | e^{-Ht} | \Phi(0) \rangle$. Therefore $\langle \mathcal{P} | H = 0$ must hold; upon commuting $e^{\sum_i (a_i^\dagger + b_i^\dagger)}$ with H , the creation operators are effectively shifted by 1: $a_i^\dagger \rightarrow 1 + a_i^\dagger$, $b_i^\dagger \rightarrow 1 + b_i^\dagger$. The probability conservation condition is thus satisfied provided $H_i(a_i^\dagger \rightarrow 1, b_i^\dagger \rightarrow 1; a_i, b_i) = 0$, which is of course true for our explicit expressions (9) and (10). Through this prescription, we may replace $a_i^\dagger a_i \rightarrow a_i$ and $b_i^\dagger b_i \rightarrow b_i$ in all averages; e.g., the predator and prey densities become $a(t) = \langle a_i(t) \rangle$ and $b(t) = \langle b_i(t) \rangle$.

In the bosonic operator representation above, we have assumed that no restrictions apply to the particle occupation numbers n_i on each site. If $n_i \leq 2s + 1$, one may instead employ a representation in terms of spin s operators. An alternative approach, devised by van Wijland, utilizes the bosonic theory, but incorporates site occupation restrictions through explicit constraints, which ultimately appear as exponentials in the number operators [36]. For example, limiting the local prey occupation numbers to 0 or 1 modifies the birth process in (9) to $H_{i\sigma} = \sigma (1 - b_i^\dagger) b_i^\dagger b_i e^{-b_i^\dagger b_i}$. Instead, one could also just add a reaction that restricts the local population numbers, e.g., $B + B \rightarrow B$ with rate ν' , yielding an additional term $H_{i\nu'} = -\nu' (1 - b_i^\dagger) b_i^\dagger b_i^2$.

As a next step, we follow a well-established route in quantum many-particle theory [49] and proceed towards a field theory representation via constructing the path integral equivalent to the ‘Schrödinger’ dynamics (8) based on coherent states, which are defined as right eigenstates of the annihilation operators, $a_i |\alpha_i\rangle = \alpha_i |\alpha_i\rangle$ and $b_i |\beta_i\rangle = \beta_i |\beta_i\rangle$, labeled by their complex eigenvalues α_i and β_i . One readily confirms the explicit formula $|\alpha_i\rangle = \exp(-\frac{1}{2} |\alpha_i|^2 + \alpha_i a_i^\dagger) |0\rangle$, the overlap integral $\langle \alpha_j | \alpha_i \rangle = \exp(-\frac{1}{2} |\alpha_i|^2 - \frac{1}{2} |\alpha_j|^2 + \alpha_j^* \alpha_i)$, and the (over-)completeness relation $\int \prod_i d^2 \alpha_i |\{\alpha_i\}\rangle \langle \{\alpha_i\}| = \pi$. Splitting the temporal evolution (8) into infinitesimal increments, inserting the (over-)completeness relation at each time step, and further straightforward manipulations (details can be found in Ref. [35]) eventually yield an expression for the configurational average

$$\langle \mathcal{O}(t) \rangle \propto \int \prod_i d\alpha_i d\alpha_i^* d\beta_i d\beta_i^* \mathcal{O}(\{\alpha_i\}, \{\beta_i\}) \exp(-S[\alpha_i^*, \beta_i^*; \alpha_i, \beta_i; t]), \quad (12)$$

with an exponential statistical weight that is determined by the ‘action’

$$S[\alpha_i^*, \beta_i^*; \alpha_i, \beta_i; t] = \sum_i \left[\int_0^t dt' \left(\alpha_i^* \frac{\partial \alpha_i}{\partial t'} + \beta_i^* \frac{\partial \beta_i}{\partial t'} + H_r(\alpha_i^*, \beta_i^*; \alpha_i, \beta_i) \right) - \alpha_i(t) - \beta_i(t) - \bar{n}_0 \alpha_i^*(0) - \bar{m}_0 \beta_i^*(0) \right], \quad (13)$$

where the second term at the final time t stems from the projection states, while the last one originates in the initial Poisson distributions. Through this procedure, in the original quasi-Hamiltonian the creation and annihilation operators $a_i^\dagger(b_i^\dagger)$ and $a_i(b_i)$ are at each time instant replaced with the complex numbers $\alpha_i^*(\beta_i^*)$ and $\alpha_i(\beta_i)$.

Finally, we proceed to take the continuum limit, $\sum_i \rightarrow a_0^{-d} \int d^d x$, $\alpha_i(t) \rightarrow a_0^d a(\vec{x}, t)$, $\beta_i(t) \rightarrow a_0^d b(\vec{x}, t)$, where a_0 denotes the original microscopic lattice constant, whereupon the continuous fields a and b acquire dimensions of particle densities, and $\alpha_i^*(t) \rightarrow \hat{a}(\vec{x}, t)$, $\beta_i^*(t) \rightarrow \hat{b}(\vec{x}, t)$, such that \hat{a} and \hat{b} remain dimensionless. The ‘bulk’ part of the action then becomes

$$S[\hat{a}, \hat{b}; a, b] = \int d^d x \int dt \left[\hat{a} \left(\frac{\partial}{\partial t} - D_A \nabla^2 \right) a + \hat{b} \left(\frac{\partial}{\partial t} - D_B \nabla^2 \right) b + H_r(\hat{a}, \hat{b}; a, b) \right], \quad (14)$$

where the discrete hopping contribution (10) has turned into a continuum diffusion term, with diffusivities $D_{A/B} = a_0^2 D'_{A/B}$. We have thus arrived at a (mesoscopic) field theory for stochastic reaction-diffusion processes, with its dynamics governed by two independent fields for each particle species, without invoking any assumptions on the form of the internal reaction noise. For the Lotka–Volterra reactions (1) with site occupation number restrictions and/or population-limiting reactions with diffusive spreading in d spatial dimensions, the bulk action (14) reads explicitly [11]

$$S[\hat{a}, \hat{b}; a, b] = \int d^d x \int dt \left[\hat{a} \left(\frac{\partial}{\partial t} - D_A \nabla^2 \right) a + \hat{b} \left(\frac{\partial}{\partial t} - D_B \nabla^2 \right) b \right. \\ \left. + \mu(\hat{a} - 1) a - \sigma(\hat{b} - 1) \hat{b} b e^{-a_0^d \hat{b} b} + \nu(\hat{b} - 1) \hat{b} b^2 - \lambda(\hat{a} - \hat{b}) \hat{a} a b \right], \quad (15)$$

with $\nu = a_0^d \nu'$ and $\lambda = a_0^d \lambda'$; for unrestricted site occupation numbers, the exponential term just needs to be replaced with 1, and ν set to 0. Expanding $e^{-a_0^d \hat{b} b} \approx 1 - a_0^d \hat{b} b$ in the limit $a_0 \rightarrow 0$ effectively replaces the ‘hard’ exponential constraint with a ‘softened’ particle number restriction, which will henceforth be used. The action (15) may now serve as a basis for further systematic coarse-graining, constructing a perturbation expansion as described below, or, if required, a subsequent renormalization group analysis [35, 47, 48].

The associated classical field equations follow from the stationarity conditions $\delta S / \delta a = 0 = \delta S / \delta b$, which are always solved by $\hat{a} = 1 = \hat{b}$, reflecting probability conservation, and $\delta S / \delta \hat{a}(\vec{x}, t) = 0 = \delta S / \delta \hat{b}(\vec{x}, t)$, which yields precisely the mean-field rate equations augmented by diffusion terms. Setting $\hat{a} = 1 = \hat{b}$, for $a_0 = 0 = \nu$ one indeed arrives at the Lotka–Volterra rate equations (2), without any restrictions on the prey population density, plus diffusive spreading. The modified prey density equation (3) with diffusion follows instead, if either $\nu = 0$ and a ‘soft’ particle number restriction is implemented with the natural identification $\rho = a_0^{-d}$, or alternatively with $a_0 = 0$ but adding a pair coagulation reaction with rate $\nu = \sigma / \rho$. It is thus convenient to perform the field shift $\hat{a}(\vec{x}, t) = 1 + \tilde{a}(\vec{x}, t)$, $\hat{b}(\vec{x}, t) = 1 + \tilde{b}(\vec{x}, t)$, whereupon the action becomes,

$$S[\tilde{a}, \tilde{b}; a, b] = \int d^d x \int dt \left[\tilde{a} \left(\frac{\partial}{\partial t} - D_A \nabla^2 + \mu \right) a + \tilde{b} \left(\frac{\partial}{\partial t} - D_B \nabla^2 - \sigma \right) b \right. \\ \left. - \sigma \tilde{b}^2 b + \frac{\sigma}{\rho} (1 + \tilde{b})^\alpha \tilde{b} b^2 - \lambda (1 + \tilde{a}) (\tilde{a} - \tilde{b}) a b \right], \quad (16)$$

with integer $\alpha = 2$ parametrizing a softened restricted prey occupation, whereas $\alpha = 1$ captures instead the presence of the binary reaction $B + B \rightarrow B$; the unrestricted model is of course recovered for $\rho \rightarrow \infty$.

We remark that for $\alpha = 1$, the action (16) is equivalent to the two coupled Langevin stochastic equations of motion

$$\begin{aligned}\frac{\partial a(\vec{x}, t)}{\partial t} &= (D_A \nabla^2 - \mu) a(\vec{x}, t) + \lambda a(\vec{x}, t) b(\vec{x}, t) + \zeta(\vec{x}, t) , \\ \frac{\partial b(\vec{x}, t)}{\partial t} &= (D_B \nabla^2 + \sigma) b(\vec{x}, t) - \frac{\sigma}{\rho} b(\vec{x}, t)^2 - \lambda a(\vec{x}, t) b(\vec{x}, t) + \eta(\vec{x}, t) ,\end{aligned}\tag{17}$$

i.e., the diffusive rate equations for the local particle densities, with added Gaussian white noise with vanishing means, $\langle \zeta \rangle = 0 = \langle \eta \rangle$, and the (cross-)correlations

$$\begin{aligned}\langle \zeta(\vec{x}, t) \zeta(\vec{x}', t') \rangle &= 2\lambda a(\vec{x}, t) b(\vec{x}, t) \delta(\vec{x} - \vec{x}') \delta(t - t') , \\ \langle \zeta(\vec{x}, t) \eta(\vec{x}', t') \rangle &= -\lambda a(\vec{x}, t) b(\vec{x}, t) \delta(\vec{x} - \vec{x}') \delta(t - t') , \\ \langle \eta(\vec{x}, t) \eta(\vec{x}', t') \rangle &= 2\sigma b(\vec{x}, t) \left[1 - b(\vec{x}, t)/\rho \right] \delta(\vec{x} - \vec{x}') \delta(t - t') ,\end{aligned}\tag{18}$$

describing multiplicative noise terms that vanish with the particle densities, as appropriate for the absorbing state at $a = 0 = b$. The equivalence of eqs. (17) and (18) with the action (16) follows immediately from the standard Janssen–De Dominicis field theory representation of Langevin dynamics [50, 51] (see also Refs. [47, 48]), according to which the set of Langevin equations $\partial s_i(\vec{x}, t)/\partial t = F_i[\{s_i(\vec{x}, t)\}] + \zeta_i(\vec{x}, t)$ with $\langle \zeta_i \rangle = 0$ and noise correlations $\langle \zeta_i(\vec{x}, t) \zeta_j(\vec{x}', t') \rangle = 2L_{ij}[\{s_i(\vec{x}, t)\}] \delta(\vec{x} - \vec{x}') \delta(t - t')$ is governed by the action

$$S[\{\tilde{s}_i\}; \{s_i\}] = \int d^d x \int dt \sum_i \left[\tilde{s}_i \left(\frac{\partial s_i}{\partial t} - F_i[\{s_i\}] \right) - \sum_j \tilde{s}_i L_{ij}[\{s_i\}] \tilde{s}_j \right] . \tag{19}$$

For $\alpha = 2$, the action contains a cubic term of the ‘auxiliary’ field \tilde{b} , and a direct Langevin representation is not obviously possible.

In the following, the field theory action (16) will serve as the starting point for further manipulations to (i) briefly recapitulate the identification of critical directed percolation as the universality class that governs the continuous active to absorbing state transition at the predator extinction threshold [11], and (ii) to compute the fluctuation-induced renormalization to lowest order in the predation rate for the population oscillation frequency and damping, as well as the diffusion coefficient in the two-species coexistence phase [37].

3.2. Predator extinction transition and Reggeon field theory

Here we provide the basic steps by which the effective field theory that describes the universal scaling behavior near the predator extinction threshold is constructed, following Ref. [11]. For $\lambda \approx \lambda_c = \mu/\rho$, very few predators remain, while the prey almost fill the entire lattice, $a(\vec{x}, t) \approx a_r = 0$, $b(\vec{x}, t) \approx b_r = \rho$. The reaction scheme (1) is thus essentially replaced with $A \rightarrow \emptyset$ and $A \rightarrow A + A$. We then also need to add a growth-limiting process for the predator population, for example again through the binary coagulation reaction $A + A \rightarrow A$, say with rate τ ; heuristically, we have then already arrived at the standard single-species death-birth-annihilation reactions that in essence define directed percolation processes (see, e.g., Refs. [35, 41, 47, 48]).

In the Doi–Peliti representation, we consequently transform the action (16) to new fluctuating prey fields $e(\vec{x}, t) = \rho - b(\vec{x}, t)$ with vanishing mean $\langle e \rangle = 0$, and $\tilde{e}(\vec{x}, t) = -\tilde{b}(\vec{x}, t)$. With the additional predator pair coagulation reaction, this yields

$$\begin{aligned} S[\tilde{a}, \tilde{e}; a, e] = & \int d^d x \int dt \left[\tilde{a} \left(\frac{\partial}{\partial t} - D_A \nabla^2 + \mu - \lambda \rho \right) a + \tau \tilde{a} (1 + \tilde{a}) a^2 \right. \\ & + \tilde{e} \left(\frac{\partial}{\partial t} - D_B \nabla^2 + \sigma \right) e - \sigma \left[(1 - \tilde{e})^\alpha - 1 \right] \tilde{e} (\rho - 2e) - \frac{\sigma}{\rho} (1 - \tilde{e})^\alpha \tilde{e} e^2 \\ & \left. - \lambda \rho (\tilde{a}^2 + (1 + \tilde{a}) \tilde{e}) a + \lambda (1 + \tilde{a}) (\tilde{a} + \tilde{e}) a e \right]. \quad (20) \end{aligned}$$

Next we note that the birth rate is a relevant parameter in the renormalization group sense, which scales to infinity under scale transformations; this observation simply expresses the fact that fluctuations of the nearly uniform prey population become strongly suppressed through the ‘mass’ term $\propto \sigma$ for the e fields. It is therefore appropriate to introduce rescaled fields $\phi(\vec{x}, t) = \sqrt{\sigma} e(\vec{x}, t)$ and $\tilde{\phi}(\vec{x}, t) = \sqrt{\sigma} \tilde{e}(\vec{x}, t)$, and subsequently take the limit $\sigma \rightarrow \infty$, which yields the much reduced effective action

$$\begin{aligned} S_\infty[\tilde{a}, \tilde{\phi}; a, \phi] = & \int d^d x \int dt \left[\tilde{a} \left(\frac{\partial}{\partial t} - D_A \nabla^2 + \mu - \lambda \rho \right) a - \lambda \rho \tilde{a}^2 a \right. \\ & \left. + \tau \tilde{a} (1 + \tilde{a}) a^2 + \tilde{\phi} \phi + \alpha \rho \tilde{\phi}^2 \right]. \quad (21) \end{aligned}$$

Since the fields ϕ and $\tilde{\phi}$ only appear as a bilinear form in the action (21), they can readily be integrated out, leaving

$$S'_\infty[\tilde{\psi}, \psi] = \int d^d x \int dt \left[\tilde{\psi} \left(\frac{\partial}{\partial t} + D_A (r_A - \nabla^2) \right) \psi - u \tilde{\psi} (\tilde{\psi} - \psi) \psi + \tau \tilde{\psi}^2 \psi^2 \right], \quad (22)$$

where $\psi(\vec{x}, t) = a(\vec{x}, t) \sqrt{\tau/\lambda \rho}$, $\tilde{\psi}(\vec{x}, t) = \tilde{a}(\vec{x}, t) \sqrt{\lambda \rho/\tau}$, $r_A = (\mu - \lambda \rho)/D_A$, and $u = \sqrt{\tau \lambda \rho}$. This new effective nonlinear coupling u becomes dimensionless at $d_c = 4$, signifying the upper critical dimension for this field theory. Near four dimensions, the quartic term $\propto \tau$ constitutes an irrelevant contribution in the renormalization group sense and may be omitted for the analysis of universal asymptotic power laws at the phase transition. The action (22) then becomes identical to Reggeon field theory, which is known to describe the critical scaling exponents for directed percolation [38]–[41]. This mapping to Reggeon field theory hence confirms the general expectation that the predator extinction threshold is governed by the directed percolation universality class [9, 10], [13]–[16], [18, 19], which features quite prominently in phase transitions to absorbing states [40, 42], even in multi-species systems [44]. The universal scaling properties of critical directed percolation are well-understood and quantitatively characterized to remarkable accuracy, both numerically through extensive Monte Carlo simulations and analytically by means of renormalization group calculations (for overviews, see Refs. [43, 45, 41]).

4. Fluctuation corrections in the coexistence phase

We now proceed to investigate and analyze the effect of intrinsic stochastic fluctuations and spatial correlations in the two-species coexistence phase, expanding about the (undamped) mean-field theory with infinite prey carrying capacity, $\rho \rightarrow \infty$.

4.1. Doi–Peliti action in the two-species coexistence phase

In order to address fluctuation corrections in the predator–prey coexistence phase [37], we start again from the Doi–Peliti field theory action (16), and introduce proper fluctuating fields $c(\vec{x}, t) = a(\vec{x}, t) - \langle a \rangle$ and $d(\vec{x}, t) = b(\vec{x}, t) - \langle b \rangle$ with vanishing mean:

$$a(\vec{x}, t) = \frac{\sigma}{\lambda} \left(1 - \frac{\mu}{\rho \lambda} + A_c \right) + c(\vec{x}, t), \quad b(\vec{x}, t) = \frac{\mu}{\lambda} (1 + B_c) + d(\vec{x}, t). \quad (23)$$

Here, the mean-field values for the stationary densities have been taken into account already, such that the counter-terms A_c and B_c , which are naturally determined by the conditions $\langle c \rangle = 0 = \langle d \rangle$, contain only fluctuation contributions; this is in accord with standard procedures for perturbation expansions in ordered phases [52]–[54]. Upon inserting (23) into (16), and renaming $\tilde{a}(\vec{x}, t) = \tilde{c}(\vec{x}, t)$ and $\tilde{b}(\vec{x}, t) = \tilde{d}(\vec{x}, t)$, one arrives at the action $S[\tilde{c}, \tilde{d}; c, d]$ in terms of the new fields. It is a sum of three contributions,

$$\begin{aligned} S_s[\tilde{c}, \tilde{d}; c, d] = & -\frac{\sigma \mu}{\lambda} \int d^d x \int dt \left[B_c \left(1 - \frac{\mu}{\rho \lambda} + A_c \right) \tilde{c} \right. \\ & - (1 + B_c) \left(A_c + \frac{\mu}{\rho \lambda} B_c \right) \tilde{d} + \left(1 - \frac{\mu}{\rho \lambda} + A_c \right) (1 + B_c) \tilde{c} (\tilde{c} - \tilde{d}) \\ & \left. + (1 + B_c) \left[1 - \alpha \frac{\mu}{\rho \lambda} (1 + B_c) \right] \tilde{d}^2 - (\alpha - 1) \frac{\mu}{\rho \lambda} (1 + B_c)^2 \tilde{d}^3 \right], \end{aligned} \quad (24)$$

which represent source terms, the bilinear or harmonic contributions

$$\begin{aligned} S_h[\tilde{c}, \tilde{d}; c, d] = & \int d^d x \int dt \left[\tilde{c} \left(\frac{\partial}{\partial t} - D_A \nabla^2 - \mu B_c \right) c + \mu (1 + B_c) \tilde{d} c \right. \\ & \left. - \sigma \left(1 - \frac{\mu}{\rho \lambda} + A_c \right) \tilde{c} d + \tilde{d} \left(\frac{\partial}{\partial t} - D_B \nabla^2 + \sigma \left[A_c + \frac{\mu}{\rho \lambda} (1 + 2B_c) \right] \right) d \right], \end{aligned} \quad (25)$$

and finally the nonlinear vertices

$$\begin{aligned} S_v[\tilde{c}, \tilde{d}; c, d] = & - \int d^d x \int dt \left[\mu (1 + B_c) \tilde{c} (\tilde{c} - \tilde{d}) c \right. \\ & + \sigma \left(1 - \frac{\mu}{\rho \lambda} + A_c \right) \tilde{c} (\tilde{c} - \tilde{d}) d + \sigma \left[1 - 2\alpha \frac{\mu}{\rho \lambda} (1 + B_c) \right] \tilde{d}^2 d \\ & \left. - 2(\alpha - 1) \frac{\sigma \mu}{\rho \lambda} (1 + B_c) \tilde{d}^3 d + \lambda (1 + \tilde{c}) (\tilde{c} - \tilde{d}) c d - \frac{\sigma}{\rho} (1 + \tilde{d})^\alpha \tilde{d} d^2 \right] \end{aligned} \quad (26)$$

(recall that the exclusion parameter assumes only the values $\alpha = 1$ or 2). Note that since the definitions (23) already contain the mean-field expectation values of the field, the linear source terms $\sim \tilde{c}, \tilde{d}$ in (24) are mere counter-terms.

The integrand in the harmonic action (25) can be written as a bilinear form $(\tilde{c} \ \tilde{d}) \bar{A} \begin{pmatrix} c \\ d \end{pmatrix}$. Defining the spatial and temporal Fourier transform for an arbitrary field via

$$\phi(\vec{x}, t) = \int \frac{d^d q}{(2\pi)^d} \int \frac{d\omega}{2\pi} \phi(\vec{q}, \omega) e^{i(\text{vec} \vec{q} \cdot \vec{x} - \omega t)}, \quad (27)$$

(and omitting the fluctuation corrections $\sim A_c, B_c$), we have in Fourier space

$$\bar{A}(q, \omega) = \begin{pmatrix} -i\omega + D_A q^2 & -\sigma(1 - \mu/\rho\lambda) \\ \mu & -i\omega + D_B q^2 + \sigma\mu/\rho\lambda \end{pmatrix}. \quad (28)$$

The next step is to diagonalize the non-symmetric bilinear coupling matrix $\bar{A} = \bar{A}(0, 0)$. To this end, we need its right and left eigenvectors, $\bar{A} e_{\pm} = \bar{\lambda}_{\pm} e_{\pm}$, $f_{\pm}^T \bar{A} = \bar{\lambda}_{\pm} f_{\pm}^T$ that satisfy the orthogonality relation $f_{\pm}^T e_{\mp} = 0$. Introducing the eigenvector matrices $P = (e_+ \ e_-)$ and $Q = (f_+ \ f_-)$, one then readily confirms $Q^T \bar{A} P = \text{diag}(\lambda_+ \ \lambda_-)$, with the diagonal elements $\lambda_{\pm} = \bar{\lambda}_{\pm} f_{\pm}^T e_{\pm}$. Upon defining new fields φ_{\pm} and $\tilde{\varphi}_{\pm}$ via $\begin{pmatrix} c \\ d \end{pmatrix} = P \begin{pmatrix} \varphi_+ \\ \varphi_- \end{pmatrix}$ and $(\tilde{c} \ \tilde{d}) = (\tilde{\varphi}_+ \ \tilde{\varphi}_-) Q^T$, finally $(\tilde{c} \ \tilde{d}) \bar{A} \begin{pmatrix} c \\ d \end{pmatrix} = (\tilde{\varphi}_+ \ \tilde{\varphi}_-) \text{diag}(\lambda_+, \lambda_-) \begin{pmatrix} \varphi_+ \\ \varphi_- \end{pmatrix} = \lambda_+ \tilde{\varphi}_+ \varphi_+ + \lambda_- \tilde{\varphi}_- \varphi_-$. The eigenvalues of the matrix \bar{A} are just the negative of the stability matrix eigenvalues in the coexistence phase, $\bar{\lambda}_{\pm} = \pm i\omega_0 + \gamma_0 = -\epsilon_{\pm}$, c.f. eq. (4), with the mean-field (‘bare’) oscillation frequency ω_0 and damping constant γ_0 (see also Ref. [46]):

$$\omega_0^2 = \mu \sigma \left(1 - \frac{\mu}{\rho\lambda}\right) - \gamma_0^2, \quad \gamma_0 = \frac{\mu \sigma}{2\rho\lambda}. \quad (29)$$

Observe that $\omega_0^2 = \mu \sigma$ and $\gamma_0 \rightarrow 0$ as the carrying capacity $\rho \rightarrow \infty$: There is no damping of the mean-field oscillations in the absence of local particle number restrictions; in this situation, damping terms are in fact generated by stochastic fluctuations, as will be demonstrated below. Choosing the eigenvectors $e_{\pm}^T = (i\omega_0 \mp \gamma_0 \pm \mu)/i\omega_0\sqrt{2\mu}$, $f_{\pm}^T = (\pm\mu \ i\omega_0 \pm \gamma_0)/i\omega_0\sqrt{2\mu}$, with $f_{\pm}^T e_{\pm} = \pm 1/i\omega_0$, the harmonic action (25) is diagonalized by means of the linear field transformations

$$\begin{aligned} c &= \frac{1}{\sqrt{2\mu}} \left(\varphi_+ + \varphi_- - \gamma_0 \frac{\varphi_+ - \varphi_-}{i\omega_0} \right), \quad d = \sqrt{\frac{\mu}{2}} \frac{\varphi_+ - \varphi_-}{i\omega_0} \\ \tilde{c} &= \sqrt{\frac{\mu}{2}} \frac{\tilde{\varphi}_+ - \tilde{\varphi}_-}{i\omega_0}, \quad \tilde{d} = \frac{1}{\sqrt{2\mu}} \left(\tilde{\varphi}_+ + \tilde{\varphi}_- + \gamma_0 \frac{\tilde{\varphi}_+ - \tilde{\varphi}_-}{i\omega_0} \right). \end{aligned} \quad (30)$$

Indeed, upon inserting (30) into (25), one obtains the harmonic action in terms of the new fields

$$\begin{aligned} S_h[\tilde{\varphi}_{\pm}; \varphi_{\pm}] &= \frac{1}{i\omega_0} \int d^d x \int dt \left[\tilde{\varphi}_+ \left(\frac{\partial}{\partial t} - D_0 \nabla^2 + \frac{\gamma_0}{i\omega_0} D'_0 \nabla^2 + i\omega_0 + \gamma_0 \right. \right. \\ &\quad \left. \left. + \frac{i\omega_0 + \gamma_0 - \mu}{2i\omega_0} \sigma A_c + \frac{(i\omega_0 - \gamma_0)(i\omega_0 + \gamma_0 - \mu) + 4\gamma_0(i\omega_0 + \gamma_0)}{2i\omega_0} B_c \right) \varphi_+ \right. \\ &\quad \left. - \tilde{\varphi}_+ \left(\frac{i\omega_0 + \gamma_0}{i\omega_0} D'_0 \nabla^2 + \frac{i\omega_0 + \gamma_0 - \mu}{2i\omega_0} \sigma A_c - \frac{(i\omega_0 + \gamma_0)(i\omega_0 - 3\gamma_0 - \mu)}{2i\omega_0} B_c \right) \varphi_- \right. \\ &\quad \left. + \tilde{\varphi}_- \left(\frac{i\omega_0 - \gamma_0}{i\omega_0} D'_0 \nabla^2 + \frac{i\omega_0 - \gamma_0 + \mu}{2i\omega_0} \sigma A_c + \frac{(i\omega_0 - \gamma_0)(i\omega_0 + 3\gamma_0 + \mu)}{2i\omega_0} B_c \right) \varphi_+ \right] \end{aligned}$$

$$\begin{aligned}
& -\tilde{\varphi}_- \left(\frac{\partial}{\partial t} - D_0 \nabla^2 - \frac{\gamma_0}{i\omega_0} D'_0 \nabla^2 - i\omega_0 + \gamma_0 + \frac{i\omega_0 - \gamma_0 + \mu}{2i\omega_0} \sigma A_c \right. \\
& \quad \left. - \frac{(i\omega_0 + \gamma_0)(i\omega_0 - \gamma_0 + \mu) - 4\gamma_0(i\omega_0 - \gamma_0)}{2i\omega_0} B_c \right) \varphi_- \Big], \quad (31)
\end{aligned}$$

where $D_0 = (D_A + D_B)/2$ denotes the mean particle diffusivity, and $D'_0 = (D_A - D_B)/2$ indicates the asymmetry in the diffusion coefficients. In the following, we shall restrict ourselves to the case of equal diffusivities $D_A = D_B = D_0$ and $D'_0 = 0$; the harmonic propagators in the diagonalized theory then read in Fourier space

$$\langle \tilde{\varphi}_\pm(\vec{q}, \omega) \varphi_\pm(\vec{q}', \omega') \rangle_0 = \frac{\pm i\omega_0}{-i\omega + D_0 q^2 \pm i\omega_0 + \gamma_0} (2\pi)^{d+1} \delta(\vec{q} + \vec{q}') \delta(\omega + \omega'), \quad (32)$$

whereas the off-diagonal two-point correlation functions $\langle \tilde{\varphi}_\pm(\vec{q}, \omega) \varphi_\mp(\vec{q}', \omega') \rangle$ contain only counter-terms and hence vanish in the harmonic approximation. Akin to spin waves in magnets, the poles of the propagators (32) describe (anti-)clockwise propagating waves with frequency ω_0 and damping γ_0 , with additional diffusive relaxation $\sim D_0 q^2$. The delta functions in (32) reflect spatial and temporal time translation invariance.

Upon expressing the sources (24) and nonlinear contributions (26) as functionals of the new fields, a multitude of terms is generated which renders any subsequent analysis quite cumbersome, see Appendix A. Consequently we shall address the limit of large prey carrying capacity $\rho \rightarrow \infty$, for which the mean-field approximation predicts undamped oscillatory modes with frequency $\omega_0 = \sqrt{\mu\sigma}$, see eq. (4). Correspondingly, we shall henceforth retain finite ρ and non-zero damping γ_0 solely in the propagator terms (31), but set $\rho^{-1} = 0 = \gamma_0$ everywhere else. The source terms then just read

$$\begin{aligned}
S_s[\tilde{\varphi}_\pm; \varphi_\pm] = \int d^d x \int dt \Big[& \sqrt{\frac{\sigma}{2}} \frac{1}{i\lambda} \left(\left[i\omega_0 A_c (1 + B_c) - \mu B_c (1 + A_c) \right] \tilde{\varphi}_+ \right. \\
& \quad \left. + \left[i\omega_0 A_c (1 + B_c) + \mu B_c (1 + A_c) \right] \tilde{\varphi}_- \right) \\
& - \frac{1 + B_c}{2\lambda} \left(\left[(i\omega_0 - \mu) (1 + A_c) + \sigma \right] \tilde{\varphi}_+^2 \right. \\
& \quad \left. + 2 \left[\mu (1 + A_c) + \sigma \right] \tilde{\varphi}_+ \tilde{\varphi}_- - \left[(i\omega_0 + \mu) (1 + A_c) - \sigma \right] \tilde{\varphi}_-^2 \right) \Big], \quad (33)
\end{aligned}$$

compare (A.1) in Appendix A. The linear source terms are mere counter-terms; following eq. (19), one may interpret the quadratic ones as generated by stochastic noise.

From eq. (26) one obtains the three-point vertices in the limit $\rho \rightarrow \infty$:

$$\begin{aligned}
S_v[\tilde{\varphi}_\pm; \varphi_\pm] = \frac{1}{2\sqrt{2\mu}\omega_0^2} \int d^d x \int dt \Big[& \left((i\omega_0 - \mu) \left[i\omega_0 (1 + A_c) - \mu (1 + B_c) \right] \right. \\
& \quad \left. + i\omega_0 \sigma \right) \tilde{\varphi}_+^2 \varphi_+ \\
& - \left((i\omega_0 - \mu) \left[i\omega_0 (1 + A_c) + \mu (1 + B_c) \right] + i\omega_0 \sigma \right) \tilde{\varphi}_+^2 \varphi_- \\
& + 2 \left(\mu \left[i\omega_0 (1 + A_c) - \mu (1 + B_c) \right] + i\omega_0 \sigma \right) \tilde{\varphi}_+ \tilde{\varphi}_- \varphi_+ \\
& \quad \left. + 2 \left(\mu \left[i\omega_0 (1 + A_c) + \mu (1 + B_c) \right] + i\omega_0 \sigma \right) \tilde{\varphi}_+ \tilde{\varphi}_- \varphi_- \right]
\end{aligned}$$

$$\begin{aligned}
& -2 \left(\mu \left[i\omega_0 (1 + A_c) + \mu (1 + B_c) \right] + i\omega_0 \sigma \right) \tilde{\varphi}_+ \tilde{\varphi}_- \varphi_- \\
& - \left((i\omega_0 + \mu) \left[i\omega_0 (1 + A_c) - \mu (1 + B_c) \right] - i\omega_0 \sigma \right) \tilde{\varphi}_-^2 \varphi_+ \\
& + \left((i\omega_0 + \mu) \left[i\omega_0 (1 + A_c) + \mu (1 + B_c) \right] - i\omega_0 \sigma \right) \tilde{\varphi}_-^2 \varphi_- \\
& - \lambda (i\omega_0 - \mu) \tilde{\varphi}_+ (\varphi_+^2 - \varphi_-^2) - \lambda (i\omega_0 + \mu) \tilde{\varphi}_- (\varphi_+^2 - \varphi_-^2) \Big]. \quad (34)
\end{aligned}$$

The nonlinear vertices of the full action are listed in eqs. (A.2), (A.3) in Appendix A. Note that in the large carrying capacity approximation, the various field theory contributions naturally become independent of the parameter α . Both the reduced and full actions remain essentially invariant under exchange of the labels $+$ \longleftrightarrow $-$, aside from complex conjugation, an obvious consequence of the complex conjugate eigenvalue pairs $\bar{\lambda}_\pm$ for \bar{A} and the corresponding eigenvector symmetry, see eq. (30). Formally, this symmetry is conveniently expressed in terms the vertex functions with m_\pm external outgoing $\tilde{\varphi}_\pm$ and n_\pm incoming φ_\pm legs:

$$\Gamma_{+^{m_+} -^{m_-}; +^{n_+} -^{n_-}}(\vec{x}_i, t_i) = \Gamma_{+^{m_-} -^{m_+}; +^{n_-} -^{n_+}}(\vec{x}_i, t_i)^* . \quad (35)$$

As a direct consequence, $\Gamma_{+^{m_-} -^{m_+}; +^{n_-} -^{n_+}}(\vec{x}_i, t_i)$ must be real.

4.2. Counter-terms and propagator renormalization to one-loop order

The propagators (32) along with two two-point noise sources (33) and three-point vertices (34) represent the building blocks for the Feynman diagrams that graphically represent the different contributions in a perturbation expansion with respect to the predation rate λ , which serves as the nonlinear coupling here [37].

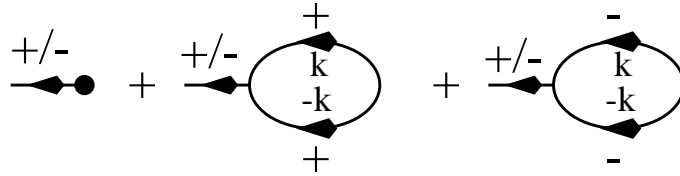


Figure 1. Feynman graphs for the expectation values $\langle \varphi_\pm \rangle$ up to one-loop order, where the ‘•’ symbol in the first diagram represents the counter-terms.

As our first step, we need to determine the counter-terms A_c and B_c to first order in λ from the conditions $\langle \varphi_\pm \rangle = 0$. The associated Feynman graphs are shown in Fig. 1, and the corresponding analytic expressions read

$$\begin{aligned}
0 = & \sqrt{\frac{\sigma}{2}} \frac{i}{\lambda} \left[i\omega_0 A_c \mp \mu B_c \right] \\
& + \frac{i\omega_0 \mp \mu}{4\sqrt{2\mu}} \int \frac{d^d k}{(2\pi)^d} \left(\frac{\mu - \sigma - i\omega_0}{i\omega_0 + \gamma_0 + D_0 k^2} - \frac{\mu - \sigma + i\omega_0}{-i\omega_0 + \gamma_0 + D_0 k^2} \right). \quad (36)
\end{aligned}$$

These are readily solved, with the result

$$\begin{aligned} A_c = B_c &= \frac{i\lambda}{4\omega_0} \int \frac{d^d k}{(2\pi)^d} \left(\frac{\mu - \sigma - i\omega_0}{i\omega_0 + \gamma_0 + D_0 k^2} - \frac{\mu - \sigma + i\omega_0}{-i\omega_0 + \gamma_0 + D_0 k^2} \right) + O(\lambda^2) \\ &= \frac{\lambda}{2} \int \frac{d^d k}{(2\pi)^d} \frac{\mu - \sigma + \gamma_0 + D_0 k^2}{\omega_0^2 + (\gamma_0 + D_0 k^2)^2} + O(\lambda^2). \end{aligned} \quad (37)$$

We may now proceed to the fluctuation renormalization of the propagators (32) to first order in the predation rate λ . To this end, we require the two-point vertex functions $\Gamma_{\pm;\pm}(\vec{q}, \omega)$ to one-loop order. Denoting their fluctuation corrections by $\Gamma_{\pm;\pm}^{(1)}(\vec{q}, \omega)$, the structure of the low-frequency and small-wavevector expansion is

$$\begin{aligned} \Gamma_{\pm;\pm}(\vec{q}, \omega) &= 1 + \text{Re} \Gamma_{\pm;\pm}^{(1)}(0, 0) \pm \frac{\gamma_0}{i\omega_0} + i \text{Im} \Gamma_{\pm;\pm}^{(1)}(0, 0) \pm \frac{D_0 q^2}{i\omega_0} \pm \frac{\omega}{\omega_0} \\ &\quad + q^2 \frac{\partial \Gamma_{\pm;\pm}^{(1)}(\vec{q}, 0)}{\partial q^2} \Big|_{\vec{q}=0} + i\omega \frac{\partial \Gamma_{\pm;\pm}^{(1)}(0, \omega)}{\partial i\omega} \Big|_{\omega=0} + \dots \end{aligned} \quad (38)$$

Note that the symmetry (35) implies

$$\Gamma_{+;+}(\vec{q}, 0) = \Gamma_{-;-}(\vec{q}, 0)^*, \quad \frac{\partial \Gamma_{+;+}(\vec{q}, \omega)}{\partial i\omega} \Big|_{\omega=0} = \left(\frac{\partial \Gamma_{-;-}(\vec{q}, \omega)}{\partial i\omega} \Big|_{\omega=0} \right)^*. \quad (39)$$

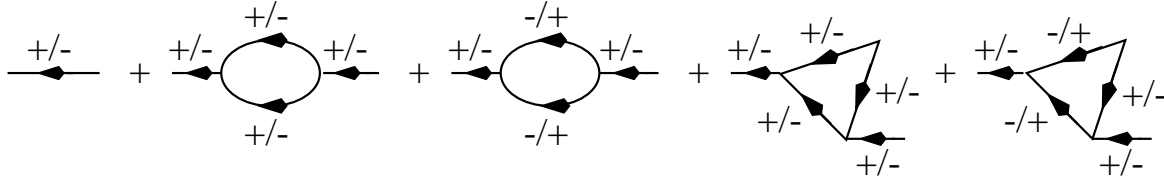


Figure 2. Feynman graphs for the vertex functions $\Gamma_{\pm;\pm}(\vec{q}, \omega)$ up to one-loop order.

The one-loop Feynman diagrams for $\Gamma_{\pm;\pm}(\vec{q}, \omega)$ are depicted in Fig. 2. Performing the internal frequency integrals, one arrives at the associated analytic expressions

$$\begin{aligned} \Gamma_{\pm;\pm}(\vec{q}, \omega) &= \frac{1}{\pm i\omega_0} \left[i\omega \pm i\omega_0 + \gamma_0 + D_0 q^2 + \left(\frac{\sigma - \mu}{2} \pm i\omega_0 \right) A_c \right] \\ &\quad + \frac{\lambda (\pm i\omega_0 - \mu)}{8 \mu \omega_0^2} [\mu (\sigma - \mu \pm 2i\omega_0) \mp i\omega_0 \sigma] \int \frac{(2\pi)^{-d} d^d k}{i\omega/2 \pm i\omega_0 + \gamma_0 + D_0 (q^2/4 + k^2)} \\ &\quad + \frac{\lambda (\pm i\omega_0 - \mu)}{8 \mu \omega_0^2} [\mu (\sigma + \mu) \pm i\omega_0 \sigma] \int \frac{(2\pi)^{-d} d^d k}{i\omega/2 \mp i\omega_0 + \gamma_0 + D_0 (q^2/4 + k^2)} \\ &\quad \pm \frac{\lambda}{8 i\omega_0} (\sigma - \mu \pm 2i\omega_0) (\sigma - \mu \pm i\omega_0) \int \frac{d^d k}{(2\pi)^d} \frac{1}{\pm i\omega_0 + \gamma_0 + D_0 (\vec{q}/2 + \vec{k})^2} \\ &\quad \times \frac{1}{\pm i\omega_0 + \gamma_0 + D_0 (\vec{q}/2 - \vec{k})^2} \frac{\pm i\omega_0 + \gamma_0 + D_0 (q^2/4 + k^2)}{i\omega/2 \pm i\omega_0 + \gamma_0 + D_0 (q^2/4 + k^2)} \\ &\quad \mp \frac{\lambda}{8 i\omega_0} (\sigma + \mu)^2 \int \frac{d^d k}{(2\pi)^d} \frac{1}{\gamma_0 + D_0 (\vec{q}/2 + \vec{k})^2} \frac{1}{\gamma_0 + D_0 (\vec{q}/2 - \vec{k})^2} \\ &\quad \times \frac{\gamma_0 + D_0 (q^2/4 + k^2)}{i\omega/2 \mp i\omega_0 + \gamma_0 + D_0 (q^2/4 + k^2)}, \end{aligned} \quad (40)$$

where the last two terms have been symmetrized with respect to the external wavevector \vec{q} . Naturally, eq. (40) satisfies the symmetry constraints (39). Clearly, $\text{Im } \Gamma_{\pm;\pm}^{(1)}(0, 0)$ does not vanish, which implies that the nonlinear fluctuations generically either generate a damping term for the population oscillations, see eq. (42), or induce an instability towards spatial structure formation, as observed in the lattice Monte Carlo simulations.

Notice furthermore the convolution of both clock- and anti-clockwise propagating modes in the ‘triangular’ fluctuation loop of the last Feynman graph in Fig. 2. As a consequence, the imaginary ‘mass’ terms $\pm i\omega_0$ in the first two factors within the associated wavevector integral cancel each other, as becomes apparent in the final term of eq. (40). For vanishing damping $\gamma_0 \rightarrow 0$ this induces an infrared divergence in $d \leq 2$ dimensions. It is precisely these contributions that cause large fluctuation corrections for the renormalized oscillation frequency, eq. (53) below, in the coexistence phase of the spatial Lotka–Volterra system even at finite (but small) damping γ_0 .

4.3. Renormalized damping, oscillation frequency, and diffusion coefficient

Appropriate definitions of renormalized oscillation parameters are suggested by the functional form (38) of the vertex functions $\Gamma_{\pm;\pm}(\vec{q}, \omega)$. We thus cast the renormalized two-point vertex functions in the form

$$\Gamma_{\pm;\pm}^R(\vec{q}, \omega) = 1 \pm \frac{\gamma_R}{i\omega_R} \pm \frac{\omega}{\omega_R} \pm \frac{D_R q^2}{i\omega_R}, \quad (41)$$

whence we identify the renormalized damping γ_R , frequency ω_R , and diffusivity D_R via

$$\gamma_R = \frac{\gamma_0 \mp \omega_0 \text{Im } \Gamma_{\pm;\pm}^{(1)}(0, 0)}{1 \mp \omega_0 \text{Im } [\partial \Gamma_{\pm;\pm}^{(1)}(0, \omega) / \partial i\omega]_{\omega=0}}, \quad (42)$$

$$\omega_R = \frac{\omega_0 [1 + \text{Re } \Gamma_{\pm;\pm}^{(1)}(0, 0)]}{1 \mp \omega_0 \text{Im } [\partial \Gamma_{\pm;\pm}^{(1)}(0, \omega) / \partial i\omega]_{\omega=0}}, \quad (43)$$

$$D_R = \frac{D_0 \mp \omega_0 \text{Im } [\partial \Gamma_{\pm;\pm}^{(1)}(\vec{q}, 0) / \partial q^2]_{\vec{q}=0}}{1 \mp \omega_0 \text{Im } [\partial \Gamma_{\pm;\pm}^{(1)}(0, \omega) / \partial i\omega]_{\omega=0}}. \quad (44)$$

Note that a negative ‘damping’ $\gamma_R < 0$ in eq. (41) indicates an instability towards a spatially inhomogeneous configuration at wavenumber $q_c = \sqrt{|\gamma_R|/D_R}$ or characteristic wavelength $\lambda_c = 2\pi\sqrt{D_0/|\gamma_R|} + O(\lambda^2)$.

Upon collecting and rearranging the one-loop contributions in (40), one arrives at

$$\begin{aligned} \text{Re } \Gamma_{\pm;\pm}^{(1)}(0, 0) = & +\lambda \frac{\sigma - 3\mu}{8} \int \frac{d^d k}{(2\pi)^d} \frac{1}{\omega_0^2 + (\gamma_0 + D_0 k^2)^2} \\ & - \lambda \frac{(\sigma + \mu)^2}{8} \int \frac{d^d k}{(2\pi)^d} \frac{1}{\gamma_0 + D_0 k^2} \frac{1}{\omega_0^2 + (\gamma_0 + D_0 k^2)^2} \\ & - \lambda \frac{\sigma^2 - 4\sigma\mu + \mu^2}{4} \int \frac{d^d k}{(2\pi)^d} \frac{\gamma_0 + D_0 k^2}{[\omega_0^2 + (\gamma_0 + D_0 k^2)^2]^2} \\ & - \lambda \frac{3(\sigma - \mu)\sigma\mu}{4} \int \frac{d^d k}{(2\pi)^d} \frac{1}{[\omega_0^2 + (\gamma_0 + D_0 k^2)^2]^2}, \end{aligned} \quad (45)$$

$$\begin{aligned}
\mp \omega_0 \operatorname{Im} \Gamma_{\pm;\pm}^{(1)}(0,0) &= -\lambda \frac{\sigma \mu}{2} \int \frac{d^d k}{(2\pi)^d} \frac{1}{\omega_0^2 + (\gamma_0 + D_0 k^2)^2} \\
&\quad + \lambda \frac{3(\sigma - \mu) \sigma \mu}{4} \int \frac{d^d k}{(2\pi)^d} \frac{\gamma_0 + D_0 k^2}{[\omega_0^2 + (\gamma_0 + D_0 k^2)^2]^2} \\
&\quad - \lambda \frac{(\sigma^2 - 4\sigma\mu + \mu^2) \sigma \mu}{4} \int \frac{d^d k}{(2\pi)^d} \frac{1}{[\omega_0^2 + (\gamma_0 + D_0 k^2)^2]^2} .
\end{aligned} \tag{46}$$

It is worth noting that the wavevector integrals are all of order $1/k^4$ (or higher inverse powers of k) and consequently develop ultraviolet divergences only in dimensions $d \geq 4$; as they should, the counter-terms have cancelled contributions of order $1/k^2$. From eqs. (42) and (46) one immediately infers the fluctuation-induced damping

$$\begin{aligned}
\gamma_R &= \gamma_0 - \lambda \frac{\sigma \mu}{2} \int \frac{d^d k}{(2\pi)^d} \frac{1}{\omega_0^2 + (\gamma_0 + D_0 k^2)^2} \\
&\quad + \lambda \frac{3(\sigma - \mu) \sigma \mu}{4} \int \frac{d^d k}{(2\pi)^d} \frac{\gamma_0 + D_0 k^2}{[\omega_0^2 + (\gamma_0 + D_0 k^2)^2]^2} \\
&\quad - \lambda \frac{(\sigma^2 - 4\sigma\mu + \mu^2) \sigma \mu}{4} \int \frac{d^d k}{(2\pi)^d} \frac{1}{[\omega_0^2 + (\gamma_0 + D_0 k^2)^2]^2} + O(\lambda^2) .
\end{aligned} \tag{47}$$

We furthermore need

$$\begin{aligned}
\mp \omega_0 \operatorname{Im} \frac{\partial \Gamma_{\pm;\pm}^{(1)}(0,\omega)}{\partial i\omega} \Big|_{\omega=0} &= +\lambda \frac{\sigma - \mu}{8} \int \frac{d^d k}{(2\pi)^d} \frac{1}{\omega_0^2 + (\gamma_0 + D_0 k^2)^2} \\
&\quad + \lambda \frac{(\sigma + \mu)^2}{16} \int \frac{d^d k}{(2\pi)^d} \frac{1}{\gamma_0 + D_0 k^2} \frac{1}{\omega_0^2 + (\gamma_0 + D_0 k^2)^2} \\
&\quad - \lambda \frac{5\sigma^2 - 8\sigma\mu + 5\mu^2}{16} \int \frac{d^d k}{(2\pi)^d} \frac{\gamma_0 + D_0 k^2}{[\omega_0^2 + (\gamma_0 + D_0 k^2)^2]^2} \\
&\quad - \lambda \frac{13(\sigma - \mu) \sigma \mu}{16} \int \frac{d^d k}{(2\pi)^d} \frac{1}{[\omega_0^2 + (\gamma_0 + D_0 k^2)^2]^2} \\
&\quad - \lambda \frac{(\sigma + \mu)^2 \sigma \mu}{8} \int \frac{d^d k}{(2\pi)^d} \frac{1}{\gamma_0 + D_0 k^2} \frac{1}{[\omega_0^2 + (\gamma_0 + D_0 k^2)^2]^2} \\
&\quad + \lambda \frac{(\sigma^2 - 4\sigma\mu + \mu^2) \sigma \mu}{4} \int \frac{d^d k}{(2\pi)^d} \frac{\gamma_0 + D_0 k^2}{[\omega_0^2 + (\gamma_0 + D_0 k^2)^2]^3} \\
&\quad + \lambda \frac{3(\sigma - \mu) \sigma^2 \mu^2}{4} \int \frac{d^d k}{(2\pi)^d} \frac{1}{[\omega_0^2 + (\gamma_0 + D_0 k^2)^2]^3} ,
\end{aligned} \tag{48}$$

which along with (45) provides us with the renormalized oscillation frequency (43)

$$\begin{aligned}
\frac{\omega_R}{\omega_0} &= 1 - \lambda \frac{\mu}{4} \int \frac{d^d k}{(2\pi)^d} \frac{1}{\omega_0^2 + (\gamma_0 + D_0 k^2)^2} \\
&\quad - \lambda \frac{3(\sigma + \mu)^2}{16} \int \frac{d^d k}{(2\pi)^d} \frac{1}{\gamma_0 + D_0 k^2} \frac{1}{\omega_0^2 + (\gamma_0 + D_0 k^2)^2} \\
&\quad + \lambda \frac{\sigma^2 + 8\sigma\mu + \mu^2}{16} \int \frac{d^d k}{(2\pi)^d} \frac{\gamma_0 + D_0 k^2}{[\omega_0^2 + (\gamma_0 + D_0 k^2)^2]^2} \\
&\quad + \lambda \frac{(\sigma - \mu) \sigma \mu}{16} \int \frac{d^d k}{(2\pi)^d} \frac{1}{[\omega_0^2 + (\gamma_0 + D_0 k^2)^2]^2}
\end{aligned}$$

$$\begin{aligned}
& + \lambda \frac{(\sigma + \mu)^2 \sigma \mu}{8} \int \frac{d^d k}{(2\pi)^d} \frac{1}{\gamma_0 + D_0 k^2} \frac{1}{[\omega_0^2 + (\gamma_0 + D_0 k^2)^2]^2} \\
& - \lambda \frac{(\sigma^2 - 4\sigma\mu + \mu^2) \sigma \mu}{4} \int \frac{d^d k}{(2\pi)^d} \frac{\gamma_0 + D_0 k^2}{[\omega_0^2 + (\gamma_0 + D_0 k^2)^2]^3} \\
& - \lambda \frac{3(\sigma - \mu) \sigma^2 \mu^2}{4} \int \frac{d^d k}{(2\pi)^d} \frac{1}{[\omega_0^2 + (\gamma_0 + D_0 k^2)^2]^3} + O(\lambda^2), \quad (49)
\end{aligned}$$

and

$$\begin{aligned}
\mp \frac{\omega_0}{D_0} \text{Im} \left. \frac{\partial \Gamma_{\pm;\pm}^{(1)}(\vec{q}, 0)}{\partial q^2} \right|_{\vec{q}=0} & = +\lambda \frac{\sigma - \mu}{16} \int \frac{d^d k}{(2\pi)^d} \frac{1}{\omega_0^2 + (\gamma_0 + D_0 k^2)^2} \\
& + \lambda \frac{(\sigma + \mu)^2}{16} \int \frac{d^d k}{(2\pi)^d} \frac{1}{\gamma_0 + D_0 k^2} \frac{1}{\omega_0^2 + (\gamma_0 + D_0 k^2)^2} \\
& - \lambda \frac{(\sigma + \mu)^2}{8d} \int \frac{d^d k}{(2\pi)^d} \frac{D_0 k^2}{(\gamma_0 + D_0 k^2)^2} \frac{1}{\omega_0^2 + (\gamma_0 + D_0 k^2)^2} \\
& - \lambda \frac{3(\sigma - \mu)^2}{16} \int \frac{d^d k}{(2\pi)^d} \frac{\gamma_0 + D_0 k^2}{[\omega_0^2 + (\gamma_0 + D_0 k^2)^2]^2} \\
& + \lambda \frac{\sigma^2 - 4\sigma\mu + \mu^2}{8d} \int \frac{d^d k}{(2\pi)^d} \frac{D_0 k^2}{[\omega_0^2 + (\gamma_0 + D_0 k^2)^2]^2} \\
& - \lambda \frac{11(\sigma - \mu) \sigma \mu}{16} \int \frac{d^d k}{(2\pi)^d} \frac{1}{[\omega_0^2 + (\gamma_0 + D_0 k^2)^2]^2} \\
& + \lambda \frac{3(\sigma - \mu) \sigma \mu}{2d} \int \frac{d^d k}{(2\pi)^d} \frac{D_0 k^2 (\gamma_0 + D_0 k^2)}{[\omega_0^2 + (\gamma_0 + D_0 k^2)^2]^3} \\
& - \lambda \frac{(\sigma + \mu)^2 \sigma \mu}{16} \int \frac{d^d k}{(2\pi)^d} \frac{1}{\gamma_0 + D_0 k^2} \frac{1}{[\omega_0^2 + (\gamma_0 + D_0 k^2)^2]^2} \\
& + \lambda \frac{(\sigma^2 - 4\sigma\mu + \mu^2) \sigma \mu}{4} \int \frac{d^d k}{(2\pi)^d} \frac{\gamma_0 + D_0 k^2}{[\omega_0^2 + (\gamma_0 + D_0 k^2)^2]^3} \\
& - \lambda \frac{(\sigma^2 - 4\sigma\mu + \mu^2) \sigma \mu}{d} \int \frac{d^d k}{(2\pi)^d} \frac{D_0 k^2}{[\omega_0^2 + (\gamma_0 + D_0 k^2)^2]^3} \\
& + \lambda \frac{3(\sigma - \mu) \sigma^2 \mu^2}{4} \int \frac{d^d k}{(2\pi)^d} \frac{1}{[\omega_0^2 + (\gamma_0 + D_0 k^2)^2]^3} \\
& - \lambda \frac{3(\sigma - \mu) \sigma^2 \mu^2}{d} \int \frac{d^d k}{(2\pi)^d} \frac{D_0 k^2 (\gamma_0 + D_0 k^2)}{[\omega_0^2 + (\gamma_0 + D_0 k^2)^2]^4} \quad (50) \\
& + \lambda \frac{(\sigma^2 - 4\sigma\mu + \mu^2) \sigma^2 \mu^2}{d} \int \frac{d^d k}{(2\pi)^d} \frac{D_0 k^2}{[\omega_0^2 + (\gamma_0 + D_0 k^2)^2]^4},
\end{aligned}$$

whence eq. (44) with (48) at last yields the renormalized diffusion coefficient

$$\begin{aligned}
\frac{D_R}{D_0} & = 1 - \lambda \frac{\sigma - \mu}{16} \int \frac{d^d k}{(2\pi)^d} \frac{1}{\omega_0^2 + (\gamma_0 + D_0 k^2)^2} \\
& - \lambda \frac{(\sigma + \mu)^2}{8d} \int \frac{d^d k}{(2\pi)^d} \frac{D_0 k^2}{(\gamma_0 + D_0 k^2)^2} \frac{1}{\omega_0^2 + (\gamma_0 + D_0 k^2)^2} \\
& + \lambda \frac{\sigma^2 - \sigma\mu + \mu^2}{8} \int \frac{d^d k}{(2\pi)^d} \frac{\gamma_0 + D_0 k^2}{[\omega_0^2 + (\gamma_0 + D_0 k^2)^2]^2}
\end{aligned}$$

$$\begin{aligned}
& + \lambda \frac{\sigma^2 - 4\sigma\mu + \mu^2}{8d} \int \frac{d^d k}{(2\pi)^d} \frac{D_0 k^2}{[\omega_0^2 + (\gamma_0 + D_0 k^2)^2]^2} \\
& + \lambda \frac{(\sigma - \mu)\sigma\mu}{8} \int \frac{d^d k}{(2\pi)^d} \frac{1}{[\omega_0^2 + (\gamma_0 + D_0 k^2)^2]^2} \\
& + \lambda \frac{3(\sigma - \mu)\sigma\mu}{2d} \int \frac{d^d k}{(2\pi)^d} \frac{D_0 k^2 (\gamma_0 + D_0 k^2)}{[\omega_0^2 + (\gamma_0 + D_0 k^2)^2]^3} \\
& + \lambda \frac{(\sigma + \mu)^2 \sigma\mu}{16} \int \frac{d^d k}{(2\pi)^d} \frac{1}{\gamma_0 + D_0 k^2} \frac{1}{[\omega_0^2 + (\gamma_0 + D_0 k^2)^2]^2} \\
& - \lambda \frac{(\sigma^2 - 4\sigma\mu + \mu^2)\sigma\mu}{d} \int \frac{d^d k}{(2\pi)^d} \frac{D_0 k^2}{[\omega_0^2 + (\gamma_0 + D_0 k^2)^2]^3} \\
& - \lambda \frac{3(\sigma - \mu)\sigma^2\mu^2}{d} \int \frac{d^d k}{(2\pi)^d} \frac{D_0 k^2 (\gamma_0 + D_0 k^2)}{[\omega_0^2 + (\gamma_0 + D_0 k^2)^2]^4} \\
& + \lambda \frac{(\sigma^2 - 4\sigma\mu + \mu^2)\sigma^2\mu^2}{d} \int \frac{d^d k}{(2\pi)^d} \frac{D_0 k^2}{[\omega_0^2 + (\gamma_0 + D_0 k^2)^2]^4} + O(\lambda^2).
\end{aligned} \tag{51}$$

Finally, the wavevector integrals for the fluctuation corrections need to be carried out, as sketched in Appendix B. With the aid of the resulting integral table, one finds with (B.2), (B.7), and (B.9) for the renormalized or fluctuation-induced damping (47):

$$\begin{aligned}
\gamma_R &= \gamma_0 + \lambda \frac{\Gamma(1 - d/2)}{2^{d+3} \pi^{d/2}} \left(\frac{\omega_0}{D_0}\right)^{d/2} \left(\frac{\sigma}{\mu} + \frac{\mu}{\sigma}\right) \text{Im} \left(\frac{\gamma_0}{\omega_0} + i\right)^{-1+d/2} \\
&+ \lambda \frac{\Gamma(2 - d/2)}{2^{d+3} \pi^{d/2}} \left(\frac{\omega_0}{D_0}\right)^{d/2} \left[\left(\frac{\sigma}{\mu} + \frac{\mu}{\sigma} - 4\right) \text{Re} \left(\frac{\gamma_0}{\omega_0} + i\right)^{-2+d/2} \right. \\
&\quad \left. - 3 \left(\sqrt{\frac{\sigma}{\mu}} - \sqrt{\frac{\mu}{\sigma}}\right) \text{Im} \left(\frac{\gamma_0}{\omega_0} + i\right)^{-2+d/2} \right] + O(\lambda^2) \\
&= \gamma_0 + \lambda \left(\frac{\omega_0}{D_0}\right)^{d/2} \Delta \tilde{\gamma}_R + O(\lambda^2).
\end{aligned} \tag{52}$$

The renormalized oscillation frequency (49) becomes

$$\begin{aligned}
\omega_R &= \omega_0 + \lambda \frac{\Gamma(1 - d/2)}{2^{d+4} \pi^{d/2}} \left(\frac{\omega_0}{D_0}\right)^{d/2} \left[\left(\frac{\sigma}{\mu} + \frac{\mu}{\sigma} + 2\right) \text{Re} \left(\frac{\gamma_0}{\omega_0} + i\right)^{-1+d/2} \right. \\
&\quad \left. + 4 \sqrt{\frac{\sigma}{\mu}} \text{Im} \left(\frac{\gamma_0}{\omega_0} + i\right)^{-1+d/2} - \left(\frac{\sigma}{\mu} + \frac{\mu}{\sigma} + 2\right) \left(\frac{\gamma_0}{\omega_0}\right)^{-1+d/2} \right] \\
&+ \lambda \frac{\Gamma(2 - d/2)}{2^{d+4} \pi^{d/2}} \left(\frac{\omega_0}{D_0}\right)^{d/2} \left[4 \left(\sqrt{\frac{\sigma}{\mu}} - \sqrt{\frac{\mu}{\sigma}}\right) \text{Re} \left(\frac{\gamma_0}{\omega_0} + i\right)^{-2+d/2} \right. \\
&\quad \left. + \left(\frac{\sigma}{\mu} + \frac{\mu}{\sigma} - 4\right) \text{Im} \left(\frac{\gamma_0}{\omega_0} + i\right)^{-2+d/2} \right] \\
&+ \lambda \frac{\Gamma(3 - d/2)}{2^{d+5} \pi^{d/2}} \left(\frac{\omega_0}{D_0}\right)^{d/2} \left[\left(\frac{\sigma}{\mu} + \frac{\mu}{\sigma} - 4\right) \text{Re} \left(\frac{\gamma_0}{\omega_0} + i\right)^{-3+d/2} \right. \\
&\quad \left. - 3 \left(\sqrt{\frac{\sigma}{\mu}} - \sqrt{\frac{\mu}{\sigma}}\right) \text{Im} \left(\frac{\gamma_0}{\omega_0} + i\right)^{-3+d/2} \right] + O(\lambda^2) \\
&= \omega_0 + \lambda \left(\frac{\omega_0}{D_0}\right)^{d/2} \Delta \tilde{\omega}_R + O(\lambda^2),
\end{aligned} \tag{53}$$

while the renormalized diffusion coefficient (51) reads

$$\begin{aligned}
D_R &= D_0 + \lambda \frac{\Gamma(1-d/2)}{d 2^{d+3} \pi^{d/2}} \left(\frac{\omega_0}{D_0}\right)^{-1+d/2} \left(\frac{\sigma}{\mu} + \frac{\mu}{\sigma} + 2\right) \operatorname{Im} \left(\frac{\gamma_0}{\omega_0} + i\right)^{d/2} \\
&\quad - \lambda \frac{\Gamma(1-d/2)}{2^{d+4} \pi^{d/2}} \left(\frac{\omega_0}{D_0}\right)^{-1+d/2} \left(\frac{\sigma}{\mu} + \frac{\mu}{\sigma} + 2\right) \operatorname{Re} \left(\frac{\gamma_0}{\omega_0} + i\right)^{-1+d/2} \\
&\quad - \lambda \frac{\Gamma(2-d/2)}{2^{d+5} \pi^{d/2}} \left(\frac{\omega_0}{D_0}\right)^{-1+d/2} \left[2 \left(\sqrt{\frac{\sigma}{\mu}} - \sqrt{\frac{\mu}{\sigma}} \right) \operatorname{Re} \left(\frac{\gamma_0}{\omega_0} + i\right)^{-2+d/2} \right. \\
&\quad \quad \quad \left. + \left(\frac{\sigma}{\mu} + \frac{\mu}{\sigma} - 4 \right) \operatorname{Im} \left(\frac{\gamma_0}{\omega_0} + i\right)^{-2+d/2} \right] \\
&\quad + \lambda \frac{\Gamma(3-d/2)}{3 \cdot 2^{d+5} \pi^{d/2}} \left(\frac{\omega_0}{D_0}\right)^{-1+d/2} \left[\left(\frac{\sigma}{\mu} + \frac{\mu}{\sigma} - 4 \right) \operatorname{Re} \left(\frac{\gamma_0}{\omega_0} + i\right)^{-3+d/2} \right. \\
&\quad \quad \quad \left. - 3 \left(\sqrt{\frac{\sigma}{\mu}} - \sqrt{\frac{\mu}{\sigma}} \right) \operatorname{Im} \left(\frac{\gamma_0}{\omega_0} + i\right)^{-3+d/2} \right] + O(\lambda^2) \\
&= D_0 + \lambda \left(\frac{\omega_0}{D_0}\right)^{-1+d/2} \Delta \tilde{D}_R + O(\lambda^2). \tag{54}
\end{aligned}$$

Notice that the effective expansion parameter in this perturbation series is given by $(\lambda/\omega_0)(\omega_0/D_0)^{d/2}$; accordingly we have introduced dimensionless first-order fluctuation corrections $\Delta \tilde{\gamma}_R$, $\Delta \tilde{\omega}_R$, and $\Delta \tilde{D}_R$. Naturally, when diffusion is fast compared to the characteristic oscillation time scale, the system becomes well-mixed and spatial correlations irrelevant. Deviations from mean-field theory induced by the fluctuation loops are then minute. In dimensions $d < 2$, when we let $\gamma_0 \rightarrow 0$, the leading fluctuation correction to the oscillation frequency diverges $\sim (\omega_0/\gamma_0)^{1-d/2}$; it is negative, and symmetric under formal rate exchange $\mu \leftrightarrow \sigma$, c.f. the last term in the second line in eq. (53). If we interpret γ_0 in the above equations as a small, self-consistently determined damping, these features are in remarkable agreement with our earlier Monte Carlo observations: Fluctuations and correlations induced by the stochastic reaction processes induce a strong downward numerical renormalization of the oscillation frequency, with very similar functional dependence on the rates μ and σ . Note that $d_c = 2$ can be viewed as (upper) critical dimension for the appearance of singular infrared fluctuation contributions (in the limit of infinite prey carrying capacity $\rho \rightarrow \infty$ or $\gamma_0 \rightarrow 0$), which resemble dynamic coexistence anomalies induced by Goldstone modes in systems with broken continuous order parameter symmetry (see, e.g., Ref. [54] and references therein).

In the following, the expressions (52)–(54) are evaluated at integer dimensions $d = 1, 2, 3$, and 4. In low dimensions, i.e., for $d = 1$ and $d = 2$, the renormalized oscillation frequency (53) becomes singular in the limit $\gamma_0 \rightarrow 0$, caused by the interference of counter-propagating clock- and anti-clockwise internal modes. For the renormalized diffusivity D_R and the fluctuation-generated damping γ_R , these infrared singularities cancel out. In $d = 1$ dimension, the leading terms in γ_0 are:

$$\gamma_R = \gamma_0 + \frac{\lambda}{8\sqrt{2}} \sqrt{\frac{\omega_0}{D_0}} \left[1 + \frac{3}{4} \left(\sqrt{\frac{\sigma}{\mu}} - \sqrt{\frac{\mu}{\sigma}} \right) - \frac{3}{4} \left(\frac{\sigma}{\mu} + \frac{\mu}{\sigma} \right) \right] + \mathcal{O}(\lambda^2), \tag{55}$$

$$\omega_R = \omega_0 - \frac{\lambda}{16} \frac{\omega_0}{\sqrt{D_0} \gamma_0} \left[1 + \frac{1}{2} \left(\frac{\sigma}{\mu} + \frac{\mu}{\sigma} \right) \right] \quad (56)$$

$$+ \frac{11\lambda}{64\sqrt{2}} \sqrt{\frac{\omega_0}{D_0}} \left[1 - \frac{57}{44} \sqrt{\frac{\sigma}{\mu}} + \frac{25}{44} \sqrt{\frac{\mu}{\sigma}} + \frac{1}{44} \left(\frac{\sigma}{\mu} + \frac{\mu}{\sigma} \right) \right] + \mathcal{O}(\lambda^2),$$

$$D_R = D_0 + \frac{3\lambda}{64\sqrt{2}} \sqrt{\frac{D_0}{\omega_0}} \left[1 + \frac{1}{12} \left(\sqrt{\frac{\sigma}{\mu}} - \sqrt{\frac{\mu}{\sigma}} \right) + \frac{3}{4} \left(\frac{\sigma}{\mu} + \frac{\mu}{\sigma} \right) \right] + \mathcal{O}(\lambda^2). \quad (57)$$

The dimensionless fluctuation corrections $\Delta\tilde{\gamma}_R$, $\Delta\tilde{\omega}_R$, and $\Delta\tilde{D}_R$, c.f. eqs. (52)–(54),

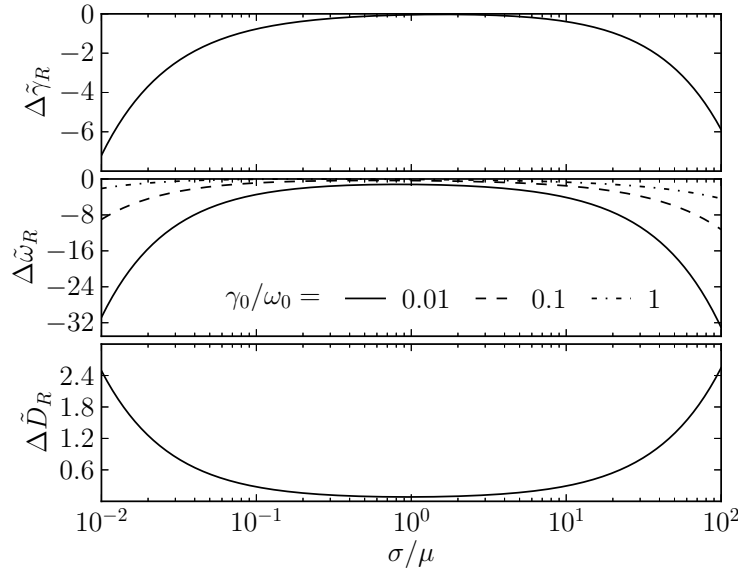


Figure 3. Fluctuation contributions to the damping $\Delta\tilde{\gamma}_R$, oscillation frequency $\Delta\tilde{\omega}_R$, and diffusivity $\Delta\tilde{D}_R$ in $d = 1$ dimension. The fluctuation corrections to the frequency depend crucially on the ratio γ_0/ω_0 , especially when $\sigma \ll \mu$ or $\sigma \gg \mu$.

are plotted in Fig. 3. The fluctuation-induced contribution to the damping is always negative, indicating the instability towards spatially inhomogeneous structures that emerge when $\gamma_0 = \lambda |\Delta\tilde{\gamma}_R| (\omega_0/D_0)^{d/2} + \mathcal{O}(\lambda^2)$. The oscillation frequency is renormalized to lower values by the loop corrections, with the leading term $\sim \sqrt{\omega_0/\gamma_0}$ further amplified when either $\sigma \ll \mu$ or $\sigma \gg \mu$. Likewise, fluctuations invariably enhance diffusive spreading. The fluctuation corrections all appear remarkably symmetric with respect to exchanging $\sigma \leftrightarrow \mu$, as is evident in Fig. 3 with its logarithmic scale for the rate ratio σ/μ by the approximate mirror symmetry about the $\sigma/\mu = 1$ axis.

In $d = 2$ dimensions, one gets

$$\gamma_R = \gamma_0 + \frac{\lambda}{64} \frac{\omega_0}{D_0} \left[\frac{6}{\pi} \left(\sqrt{\frac{\sigma}{\mu}} - \sqrt{\frac{\mu}{\sigma}} \right) - \left(\frac{\sigma}{\mu} + \frac{\mu}{\sigma} \right) \right] + \mathcal{O}(\lambda^2), \quad (58)$$

$$\omega_R = \omega_0 - \frac{\lambda}{32\pi} \frac{\omega_0}{D_0} \ln \frac{\omega_0}{\gamma_0} \cdot \left[1 + \frac{1}{2} \left(\frac{\sigma}{\mu} + \frac{\mu}{\sigma} \right) \right]$$

$$+ \frac{3\lambda}{32\pi} \frac{\omega_0}{D_0} \left[1 - \frac{\pi}{3} \sqrt{\frac{\sigma}{\mu}} - \frac{1}{4} \left(\frac{\sigma}{\mu} + \frac{\mu}{\sigma} \right) \right] + \mathcal{O}(\lambda^2), \quad (59)$$

$$D_R = D_0 + \frac{\lambda}{96\pi} \left[1 + 2 \left(\frac{\sigma}{\mu} + \frac{\mu}{\sigma} \right) \right] + \mathcal{O}(\lambda^2), \quad (60)$$

and the fluctuation contributions are depicted in Fig. 4. The graphs look remarkably alike to Fig. 3 for $d = 1$, but the overall scale of the corrections $\Delta\tilde{\gamma}_R$ and $\Delta\tilde{D}_R$ is reduced by a factor ~ 4 , and for $\Delta\tilde{\omega}_R$ by ~ 10 , with its leading term acquiring just a logarithmic singularity as $\gamma_0 \rightarrow 0$. Again, the system is rendered unstable against spatio-temporal structures. According to eq. (5), the fluctuation-enhanced diffusivity suggests faster front spreading than predicted by the bare mean-field rates, as indeed observed in two-dimensional Monte Carlo simulations [29]. The population oscillation frequency is strongly renormalized downward, with an approximately equal functional dependence on the rates σ and μ ; moreover, the deviations from the mean-field values grow in size as the ratio σ/μ is tuned away from unity. These analytic perturbative one-loop results are in remarkable agreement with the Monte Carlo simulation data for two-dimensional stochastic Lotka–Volterra systems, as shown in Fig. 9 in Ref. [11] and Fig. 6(b) in Ref. [27].

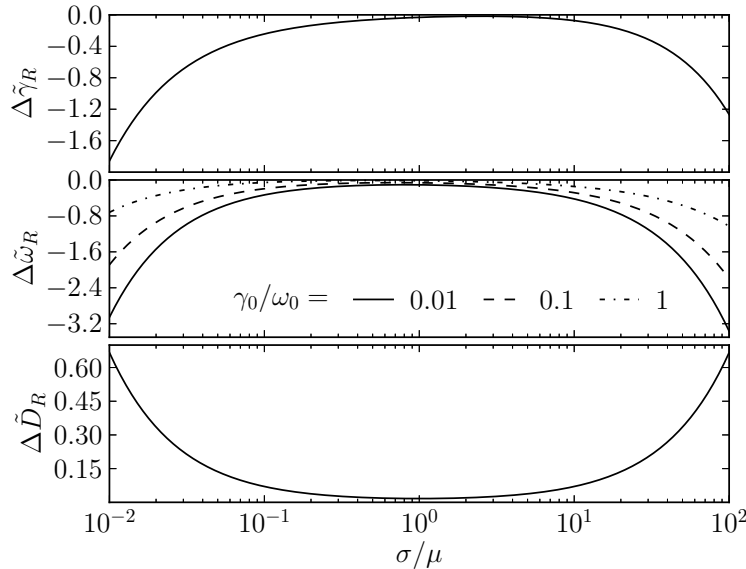


Figure 4. Fluctuation contributions to the damping $\Delta\tilde{\gamma}_R$, oscillation frequency $\Delta\tilde{\omega}_R$, and diffusivity $\Delta\tilde{D}_R$ in $d = 2$ dimensions. As in one dimension, the fluctuation corrections to the frequency strongly depend on the ratio γ_0/ω_0 .

In $d = 3$ dimensions, one may safely set the bare damping constant to zero, $\gamma_0 \rightarrow 0$ (or $\rho \rightarrow \infty$) to obtain

$$\gamma_R = \gamma_0 + \frac{\lambda(\omega_0/D_0)^{3/2}}{16\sqrt{2}\pi} \left[-1 + \frac{3}{4} \left(\sqrt{\frac{\sigma}{\mu}} - \sqrt{\frac{\mu}{\sigma}} \right) - \frac{1}{4} \left(\frac{\sigma}{\mu} + \frac{\mu}{\sigma} \right) \right] + \mathcal{O}(\lambda^2), \quad (61)$$

$$\omega_R = \omega_0 + \frac{\lambda(\omega_0/D_0)^{3/2}}{128\sqrt{2}\pi} \left[1 - \frac{13}{4} \sqrt{\frac{\sigma}{\mu}} - \frac{19}{4} \sqrt{\frac{\mu}{\sigma}} - \frac{13}{4} \left(\frac{\sigma}{\mu} + \frac{\mu}{\sigma} \right) \right] + \mathcal{O}(\lambda^2), \quad (62)$$

$$D_R = D_0 - \frac{\lambda \sqrt{\omega_0/D_0}}{384 \sqrt{2} \pi} \left[1 + \frac{9}{4} \left(\sqrt{\frac{\sigma}{\mu}} - \sqrt{\frac{\mu}{\sigma}} \right) - \frac{13}{4} \left(\frac{\sigma}{\mu} + \frac{\mu}{\sigma} \right) \right] + \mathcal{O}(\lambda^2). \quad (63)$$

Figure 5 shows the associated fluctuation corrections $\Delta\tilde{\gamma}_R$, $\Delta\tilde{\omega}_R$, and $\Delta\tilde{D}_R$, which compared to one and two dimensions are considerably reduced in magnitude, but otherwise display quite similar features.

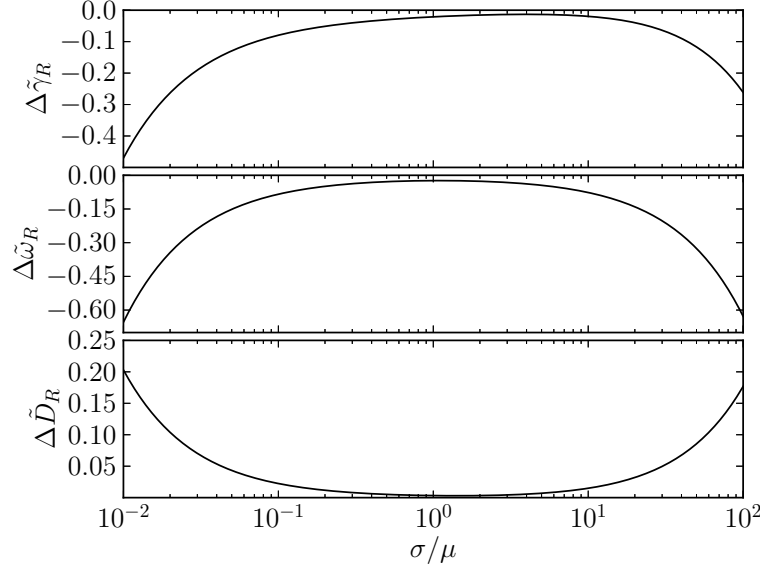


Figure 5. Fluctuation contributions to the damping $\Delta\tilde{\gamma}_R$, oscillation frequency $\Delta\tilde{\omega}_R$, and diffusivity $\Delta\tilde{D}_R$ in $d = 3$ dimensions.

In higher dimensions $d \geq 4$, the fluctuation corrections become formally ultraviolet-divergent, and thus a finite cut-off Λ in momentum space must be implemented; e.g., in $d = 4$ dimensions:

$$\gamma_R = \gamma_0 + \frac{\lambda}{32 \pi^2} \left(\frac{\omega_0}{D_0} \right)^2 \left[1 - \frac{1}{2} \ln \left(1 + \frac{\Lambda^4}{\omega_0^2/D_0^2} \right) + \frac{3 \pi}{8} \left(\sqrt{\frac{\sigma}{\mu}} - \sqrt{\frac{\mu}{\sigma}} \right) - \frac{1}{4} \left(\frac{\sigma}{\mu} + \frac{\mu}{\sigma} \right) \right] + \mathcal{O}(\lambda^2), \quad (64)$$

$$\omega_R = \omega_0 + \frac{\lambda}{256 \pi} \left(\frac{\omega_0}{D_0} \right)^2 \left[1 - \frac{2}{\pi} \sqrt{\frac{\mu}{\sigma}} \ln \left(1 + \frac{\Lambda^4}{\omega_0^2/D_0^2} \right) - \frac{5}{2 \pi^2} \left(\sqrt{\frac{\sigma}{\mu}} - \sqrt{\frac{\mu}{\sigma}} \right) - \left(\frac{\sigma}{\mu} + \frac{\mu}{\sigma} \right) \right] + \mathcal{O}(\lambda^2), \quad (65)$$

$$D_R = D_0 - \frac{\lambda}{512 \pi} \frac{\omega_0}{D_0} \left[1 + \frac{1}{\pi} \left(\sqrt{\frac{\sigma}{\mu}} - \sqrt{\frac{\mu}{\sigma}} \right) \ln \left(1 + \frac{\Lambda^4}{\omega_0^2/D_0^2} \right) - \frac{3}{\pi} \left(\sqrt{\frac{\sigma}{\mu}} - \sqrt{\frac{\mu}{\sigma}} \right) - \left(\frac{\sigma}{\mu} + \frac{\mu}{\sigma} \right) \right] + \mathcal{O}(\lambda^2). \quad (66)$$

As Fig. 6 demonstrates, the cut-off dependence in the loop corrections is rather weak in $d = 4$ dimensions. For low cut-off values, the fluctuation contributions to the damping

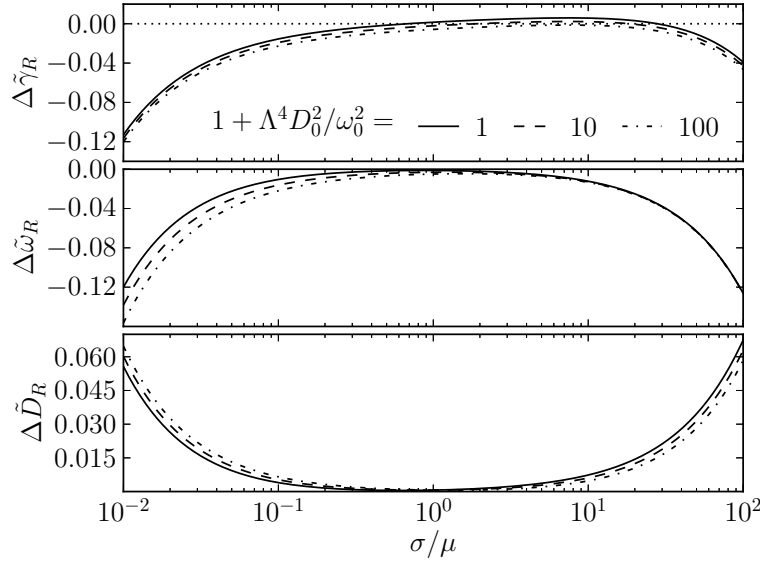


Figure 6. Fluctuation contributions to the damping $\Delta\tilde{\gamma}_R$, oscillation frequency $\Delta\tilde{\omega}_R$, and diffusivity $\Delta\tilde{D}_R$ in $d = 4$ dimensions. Notice the weak logarithmic dependence on the ultraviolet cut-off Λ .

appear positive in the approximate interval $1 \leq \sigma/\mu \leq 30$, but turn negative in the continuum limit of large Λ , still signaling instability with respect to structure formation. The typical values of $\Delta\tilde{\gamma}_R$, $\Delta\tilde{D}_R$, and $\Delta\tilde{\omega}_R$ are all diminished by factors $\sim 4 \dots 5$ as compared to $d = 3$; the cut-off dependence in the renormalized frequency only becomes noticeable for $\sigma/\mu \ll 1$, see eq. (65).

5. Conclusion and outlook

This paper describes in some detail how the stochastic kinetics of spatially extended predator-prey systems of the Lotka–Volterra type, as encoded through a classical master equation, can be mapped onto a continuum field theory representation, while faithfully preserving the internal demographic and reaction noise and the ensuing correlations. The connection of the more microscopic Doi–Peliti field theory action with a mesoscopic description in terms of coupled Langevin equations was pointed out, and the associated white noise correlations were systematically derived. The continuum representation was then employed to demonstrate that the predator extinction transition, induced by a finite prey carrying capacity, is indeed governed by the universal scaling exponents of critical directed percolation, as one would generically expect for such a nonequilibrium phase transition from an active to an absorbing state.

After a brief review of the most striking features of stochastic predator-prey models in the species coexistence phase, the Doi–Peliti field theory representation and a first-order perturbation expansion with respect to the nonlinear predation rate, in the limit of large prey carrying capacity, were employed to qualitatively and semi-

quantitatively confirm crucial salient observations from Monte Carlo simulations on regular lattices: (i) Spatial predator-prey systems in the species coexistence phase are generically characterized by the emergence of fluctuating spatial structures, namely continually expanding and merging activity fronts. (ii) The recurring passages of population waves locally incite persistent density oscillations for both predators and prey. (iii) Fluctuations in the two-species coexistence phase are remarkably and quite unusually strong; as compared with the (linearized) mean-field prediction, they considerably renormalize the oscillation frequency, especially in $d \leq 2$ dimensions. Explicit analytical results for the fluctuation-induced damping, and the renormalized oscillation frequency and diffusion coefficient were provided to one-loop order. They showed that (iv) the leading fluctuation contribution to the frequency is negative, and symmetric in its functional dependence on the rates σ and μ ; and (v) the diffusivity is invariably renormalized upward, implying faster front propagation speeds as compared to the mean-field approximation.

An important open question is which of the numerous standard mathematical models in ecology, population dynamics, and chemical kinetics, many of which are frequently analyzed merely on the level of mean-field rate equations, are similarly strongly affected by stochastic fluctuations and intrinsic correlations. Remarkably, and perhaps counter-intuitively, Monte Carlo simulations of stochastic spatial variants of cyclic three-species predator-prey systems, namely both spatial rock-paper-scissors games (with conserved total population) and the May–Leonard model (which displays no global conservation law) do not reveal noticeable fluctuation effects, see Refs. [55, 56] (and further references therein). Apparently, the mechanism causing strong fluctuations in the spatial stochastic two-species Lotka–Volterra system, namely the destructive interference of counter-propagating internal modes, is conspicuously absent in extensions to additional participating species. This fact becomes even more puzzling as the stochastic cyclic rock-paper-scissors model has been shown to reduce to the stochastic and strongly fluctuating Lotka–Volterra system in a highly asymmetric rate limit where a single species becomes abundant [57]. A careful field-theoretic analysis based on the Doi–Peliti representation of the corresponding stochastic master equation should be capable to shed light on this issue, and hopefully explain this important distinction between apparently closely related population dynamics or reaction-diffusion models.

Acknowledgments

The author is indebted to Ulrich Dobramysl for his assistance with Figs. 3–6, and gladly acknowledges helpful discussions with him, Qian He, Swapnil Jawkar, Mauro Mobilia, Michel Pleimling, Beate Schmittmann, Siddharth Venkat, and Royce Zia.

Appendix A. Field theory and counter-terms for finite carrying capacity

In this appendix, we write down the explicit field theory for finite prey carrying capacity ρ , and sketch the evaluation of the associated counter-terms A_c and B_c to first order in the predation rate λ . Upon expressing (24) in terms of the fields $\tilde{\varphi}_\pm$ and φ_\pm by means of eqs. (30), one obtains the source terms

$$\begin{aligned}
S_s[\tilde{\varphi}_\pm; \varphi_\pm] = & \int d^d x \int dt \left[\sqrt{\frac{\mu}{2}} \frac{\sigma}{i\omega_0 \lambda} \left(\left[(i\omega_0 + \gamma_0) (1 + B_c) \left(A_c + \frac{\mu}{\rho \lambda} B_c \right) - \mu B_c \times \right. \right. \right. \\
& \left. \left(1 - \frac{\mu}{\rho \lambda} + A_c \right) \right] \tilde{\varphi}_+ + \left[(i\omega_0 - \gamma_0) (1 + B_c) \left(A_c + \frac{\mu}{\rho \lambda} B_c \right) + \mu B_c \left(1 - \frac{\mu}{\rho \lambda} + A_c \right) \right] \tilde{\varphi}_- \right) \\
& + \frac{\sigma(1 + B_c)}{2\omega_0^2 \lambda} \left(\left[(i\omega_0 + \gamma_0)^2 \left(1 - \frac{\alpha \mu}{\rho \lambda} (1 + B_c) \right) - \mu(i\omega_0 + \gamma_0 - \mu) \left(1 - \frac{\mu}{\rho \lambda} + A_c \right) \right] \tilde{\varphi}_+^2 \right. \\
& \quad \left. - 2 \left[(\omega_0^2 + \gamma_0^2) \left(1 - \frac{\alpha \mu}{\rho \lambda} (1 + B_c) \right) - \mu(\gamma_0 - \mu) \left(1 - \frac{\mu}{\rho \lambda} + A_c \right) \right] \tilde{\varphi}_+ \tilde{\varphi}_- \right. \\
& \quad \left. + \left[(i\omega_0 - \gamma_0)^2 \left(1 - \frac{\alpha \mu}{\rho \lambda} (1 + B_c) \right) + \mu(i\omega_0 - \gamma_0 + \mu) \left(1 - \frac{\mu}{\rho \lambda} + A_c \right) \right] \tilde{\varphi}_-^2 \right) \\
& \quad \left. - (\alpha - 1) \sqrt{\frac{\mu}{2}} \frac{\sigma(1 + B_c)^2}{2i\omega_0^3 \rho \lambda^2} \left[(i\omega_0 + \gamma_0) \tilde{\varphi}_+ + (i\omega_0 - \gamma_0) \tilde{\varphi}_- \right]^3 \right]. \quad (\text{A.1})
\end{aligned}$$

Note that the cubic source contributions are absent if $\alpha = 1$. The nonlinear action (26) yields the three-point vertices

$$\begin{aligned}
S_v[\tilde{\varphi}_\pm; \varphi_\pm] = & -\frac{1}{2\sqrt{2\mu} i\omega_0^3} \int d^d x \int dt \left[\left((i\omega_0 + \gamma_0 - \mu) \left[(i\omega_0 - \gamma_0) \mu (1 + B_c) \right. \right. \right. \\
& \quad \left. \left. + (\omega_0^2 + \gamma_0^2 + \mu \sigma A_c) \right] - (i\omega_0 + \gamma_0)^2 \sigma \left[1 - \frac{2\alpha \mu}{\rho \lambda} (1 + B_c) \right] \right) \tilde{\varphi}_+^2 \varphi_+ \\
& \quad + \left((i\omega_0 + \gamma_0 - \mu) \left[(i\omega_0 + \gamma_0) \mu (1 + B_c) - (\omega_0^2 + \gamma_0^2 + \mu \sigma A_c) \right] \right. \\
& \quad \quad \left. + (i\omega_0 + \gamma_0)^2 \sigma \left[1 - \frac{2\alpha \mu}{\rho \lambda} (1 + B_c) \right] \right) \tilde{\varphi}_+^2 \varphi_- \\
& \quad - 2 \left((\gamma_0 - \mu) \left[(i\omega_0 - \gamma_0) \mu (1 + B_c) + (\omega_0^2 + \gamma_0^2 + \mu \sigma A_c) \right] \right. \\
& \quad \quad \left. - (\omega_0^2 + \gamma_0^2) \sigma \left[1 - \frac{2\alpha \mu}{\rho \lambda} (1 + B_c) \right] \right) \tilde{\varphi}_+ \tilde{\varphi}_- \varphi_+ \\
& \quad - 2 \left((\gamma_0 - \mu) \left[(i\omega_0 + \gamma_0) \mu (1 + B_c) - (\omega_0^2 + \gamma_0^2 + \mu \sigma A_c) \right] \right. \\
& \quad \quad \left. + (\omega_0^2 + \gamma_0^2) \sigma \left[1 - \frac{2\alpha \mu}{\rho \lambda} (1 + B_c) \right] \right) \tilde{\varphi}_+ \tilde{\varphi}_- \varphi_- \\
& \quad - \left((i\omega_0 - \gamma_0 + \mu) \left[(i\omega_0 - \gamma_0) \mu (1 + B_c) + (\omega_0^2 + \gamma_0^2 + \mu \sigma A_c) \right] \right. \\
& \quad \quad \left. + (i\omega_0 - \gamma_0)^2 \sigma \left[1 - \frac{2\alpha \mu}{\rho \lambda} (1 + B_c) \right] \right) \tilde{\varphi}_-^2 \varphi_+
\end{aligned}$$

$$\begin{aligned}
& - \left((i\omega_0 - \gamma_0 + \mu) \left[(i\omega_0 + \gamma_0) \mu (1 + B_c) - (\omega_0^2 + \gamma_0^2 + \mu \sigma A_c) \right] \right. \\
& \quad \left. - (i\omega_0 - \gamma_0)^2 \sigma \left[1 - \frac{2\alpha \mu}{\rho \lambda} (1 + B_c) \right] \right) \tilde{\varphi}_-^2 \varphi_- \\
& + \left[\lambda (i\omega_0 + \gamma_0 - \mu)(i\omega_0 - \gamma_0) + \frac{\mu \sigma}{\rho} (i\omega_0 + \gamma_0) \right] \tilde{\varphi}_+ \varphi_+^2 \\
& + 2 \left[\lambda \gamma_0 (i\omega_0 + \gamma_0 - \mu) - \frac{\mu \sigma}{\rho} (i\omega_0 + \gamma_0) \right] \tilde{\varphi}_+ \varphi_+ \varphi_- \\
& - (i\omega_0 + \gamma_0) \left[\lambda (i\omega_0 + \gamma_0 - \mu) - \frac{\mu \sigma}{\rho} \right] \tilde{\varphi}_+ \varphi_-^2 \\
& + (i\omega_0 - \gamma_0) \left[\lambda (i\omega_0 - \gamma_0 + \mu) + \frac{\mu \sigma}{\rho} \right] \tilde{\varphi}_- \varphi_+^2 \\
& + 2 \left[\lambda \gamma_0 (i\omega_0 - \gamma_0 + \mu) - \frac{\mu \sigma}{\rho} (i\omega_0 - \gamma_0) \right] \tilde{\varphi}_- \varphi_+ \varphi_- \\
& - \left[\lambda (i\omega_0 - \gamma_0 + \mu)(i\omega_0 + \gamma_0) - \frac{\mu \sigma}{\rho} (i\omega_0 - \gamma_0) \right] \tilde{\varphi}_- \varphi_-^2 \Big]. \tag{A.2}
\end{aligned}$$

In addition, there are four- and five-point vertices (the latter arise only for $\alpha = 2$):

$$\begin{aligned}
S'_v[\tilde{\varphi}_\pm; \varphi_\pm] &= \int d^d x \int dt \left[(\alpha - 1) \frac{\sigma(1 + B_c)}{2\omega_0^4 \rho \lambda} \left[(i\omega_0 + \gamma_0) \tilde{\varphi}_+ + (i\omega_0 - \gamma_0) \tilde{\varphi}_- \right]^3 (\varphi_+ - \varphi_-) \right. \\
& + \frac{\lambda}{4\omega_0^4} \left[(i\omega_0 + \gamma_0 - \mu) \tilde{\varphi}_+^2 - 2(\gamma_0 - \mu) \tilde{\varphi}_+ \tilde{\varphi}_- - (i\omega_0 - \gamma_0 + \mu) \tilde{\varphi}_-^2 \right] \times \\
& \quad \left[(i\omega_0 - \gamma_0) \varphi_+^2 + 2\gamma_0 \varphi_+ \varphi_- - (i\omega_0 + \gamma_0) \varphi_-^2 \right] \\
& + \frac{\alpha \sigma}{4\omega_0^4 \rho} \left[(i\omega_0 + \gamma_0) \tilde{\varphi}_+ + (i\omega_0 - \gamma_0) \tilde{\varphi}_- \right]^2 (\varphi_+ - \varphi_-)^2 \\
& \left. + (\alpha - 1) \frac{\sigma}{4\sqrt{2\mu} i\omega_0^5 \rho} \left[(i\omega_0 + \gamma_0) \tilde{\varphi}_+ + (i\omega_0 - \gamma_0) \tilde{\varphi}_- \right]^3 (\varphi_+ - \varphi_-)^2 \right]. \tag{A.3}
\end{aligned}$$

However, these do not enter the one-loop analysis, but only contribute to higher orders in the perturbation expansion.

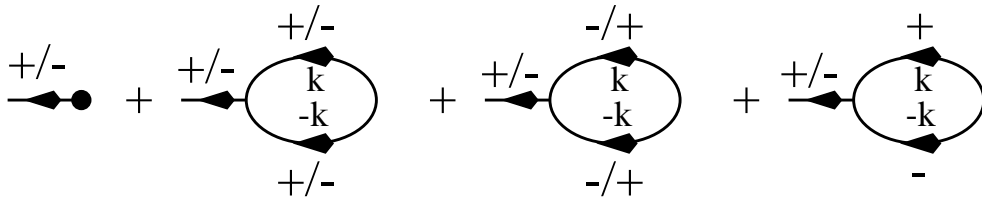


Figure A1. Feynman graphs for $\langle \varphi_\pm \rangle$ up to one-loop order in the full field theory.

Naturally, with these many contributions in the action, any subsequent perturbative calculation becomes quite elaborate and lengthy, as will next be demonstrated by computing the counter-terms A_c and B_c in the full theory. The contributing Feynman graphs up to one-loop order are depicted in Fig. A1. The associated analytic expressions

for the expectation values $\langle \varphi_{\pm} \rangle$ become to first order in λ :

$$\begin{aligned}
0 = \langle \varphi_{\pm} \rangle &= (\pm i\omega_0 + \gamma_0) \left(A_c + \frac{\mu}{\rho\lambda} B_c \right) - \mu \left(1 - \frac{\mu}{\rho\lambda} \right) B_c \\
&+ \frac{1 - \mu/\rho\lambda}{4\omega_0^2\mu} \left(\left[\lambda (\pm i\omega_0 + \gamma_0 - \mu) (\mp i\omega_0 + \gamma_0) - (\pm i\omega_0 + \gamma_0) \frac{\mu\sigma}{\rho} \right] \right. \\
&\quad \times \left[(\pm i\omega_0 + \gamma_0)^2 - \mu (\pm i\omega_0 + \gamma_0 - \mu) \right] \int \frac{(2\pi)^{-d} d^d k}{\pm i\omega_0 + \gamma_0 + D_0 k^2} \\
&\quad + (\pm i\omega_0 + \gamma_0) \left[\lambda (\pm i\omega_0 + \gamma_0 - \mu) - \frac{\mu\sigma}{\rho} \right] \\
&\quad \times \left[(\mp i\omega_0 + \gamma_0)^2 - \mu (\mp i\omega_0 + \gamma_0 - \mu) \right] \int \frac{(2\pi)^{-d} d^d k}{\mp i\omega_0 + \gamma_0 + D_0 k^2} \\
&\quad - 2 \left[\lambda \gamma_0 (\pm i\omega_0 + \gamma_0 - \mu) - (\pm i\omega_0 + \gamma_0) \frac{\mu\sigma}{\rho} \right] \\
&\quad \times \left[\omega_0^2 + \gamma_0^2 - \mu (\gamma_0 - \mu) \right] \int \frac{(2\pi)^{-d} d^d k}{\gamma_0 + D_0 k^2} \Bigg) \quad (\text{A.4}) \\
&- \frac{\alpha - 1}{4\omega_0^2\rho\lambda} \left(\left[\lambda (\pm i\omega_0 + \gamma_0 - \mu) (\mp i\omega_0 + \gamma_0) - (\pm i\omega_0 + \gamma_0) \frac{\mu\sigma}{\rho} \right] \right. \\
&\quad \times (\pm i\omega_0 + \gamma_0)^2 \int \frac{(2\pi)^{-d} d^d k}{\pm i\omega_0 + \gamma_0 + D_0 k^2} \\
&\quad + \left[\lambda (\pm i\omega_0 + \gamma_0 - \mu) - \frac{\mu\sigma}{\rho} \right] (\omega_0^2 + \gamma_0^2) (\mp i\omega_0 + \gamma_0) \int \frac{(2\pi)^{-d} d^d k}{\mp i\omega_0 + \gamma_0 + D_0 k^2} \\
&\quad \left. - 2 \left[\lambda \gamma_0 (\pm i\omega_0 + \gamma_0 - \mu) - (\pm i\omega_0 + \gamma_0) \frac{\mu\sigma}{\rho} \right] (\omega_0^2 + \gamma_0^2) \int \frac{(2\pi)^{-d} d^d k}{\gamma_0 + D_0 k^2} \right).
\end{aligned}$$

Because of the fundamental symmetry (35), separating (A.4) into its real and imaginary parts yields only two coupled linear equations for A_c and B_c . By means of straightforward (but tedious) algebra one finally obtains

$$\begin{aligned}
A_c &= -\frac{1}{2\omega_0^2\mu} \left[\left(\lambda \left[(\omega_0^2 + \gamma_0^2) (\gamma_0 - \mu) + \gamma_0 \mu^2 \right] + \frac{\mu\sigma}{\rho} \left[\omega_0^2 - \gamma_0^2 + \mu (\gamma_0 - \mu) \right] \right. \right. \\
&\quad \left. \left. - \frac{(\alpha - 1)\mu}{\rho\lambda - \mu} \left[\lambda (\omega_0^2 + \gamma_0^2) \gamma_0 + \frac{\mu\sigma}{\rho} (\omega_0^2 - \gamma_0^2) \right] \right) \int \frac{d^d k}{(2\pi)^d} \frac{\gamma_0 + D_0 k^2}{\omega_0^2 + (\gamma_0 + D_0 k^2)^2} \right. \\
&\quad \left. + \omega_0^2 \left(\lambda (\omega_0^2 + \gamma_0^2 - \mu^2) - \frac{\mu\sigma}{\rho} (2\gamma_0 - \mu) \right. \right. \\
&\quad \left. \left. - \frac{(\alpha - 1)\mu}{\rho\lambda - \mu} \left[\lambda (\omega_0^2 + \gamma_0^2) - 2 \frac{\mu\sigma}{\rho} \gamma_0 \right] \right) \int \frac{(2\pi)^{-d} d^d k}{\omega_0^2 + (\gamma_0 + D_0 k^2)^2} \right. \\
&\quad \left. - \left(\lambda \gamma_0 - \frac{\mu\sigma}{\rho} \right) \left(\omega_0^2 + \gamma_0^2 - \mu (\gamma_0 - \mu) - \frac{(\alpha - 1)\mu}{\rho\lambda - \mu} (\omega_0^2 + \gamma_0^2) \right) \int \frac{(2\pi)^{-d} d^d k}{\gamma_0 + D_0 k^2} \right] \\
&+ \frac{1}{2\omega_0^2\rho\lambda} \left[\left(2\lambda \left[\omega_0^2 (\gamma_0 - \mu) + \gamma_0 [\gamma_0^2 - \mu (\gamma_0 - \mu)] \right] + \frac{\mu\sigma}{\rho} \left[\omega_0^2 - \gamma_0^2 + \mu (\gamma_0 - \mu) \right] \right. \right. \\
&\quad \left. \left. - \frac{(\alpha - 1)\mu}{\rho\lambda - \mu} \left[2\lambda (\omega_0^2 + \gamma_0^2) \gamma_0 + \frac{\mu\sigma}{\rho} (\omega_0^2 - \gamma_0^2) \right] \right) \int \frac{d^d k}{(2\pi)^d} \frac{\gamma_0 + D_0 k^2}{\omega_0^2 + (\gamma_0 + D_0 k^2)^2} \right. \\
&\quad \left. + \omega_0^2 \left(2\lambda (\omega_0^2 + \gamma_0^2 - \mu^2) - \frac{\mu\sigma}{\rho} (2\gamma_0 - \mu) \right) \right.
\end{aligned} \quad (\text{A.5})$$

$$- \frac{2(\alpha-1)\mu}{\rho\lambda-\mu} \left[\lambda(\omega_0^2 + \gamma_0^2) - \frac{\mu\sigma}{\rho} \gamma_0 \right] \int \frac{(2\pi)^{-d} d^d k}{\omega_0^2 + (\gamma_0 + D_0 k^2)^2} \\ - \left(2\lambda\gamma_0 - \frac{\mu\sigma}{\rho} \right) \left(\omega_0^2 + \gamma_0^2 - \mu(\gamma_0 - \mu) - \frac{(\alpha-1)\mu}{\rho\lambda-\mu} (\omega_0^2 + \gamma_0^2) \right) \int \frac{(2\pi)^{-d} d^d k}{\gamma_0 + D_0 k^2} \Big],$$

and

$$B_c = -\frac{\lambda}{2\omega_0^2\mu} \left(\left[\omega_0^2(\gamma_0 - \mu) + \gamma_0[\gamma_0^2 - \mu(\gamma_0 - \mu)] \right. \right. \\ \left. \left. - \frac{(\alpha-1)\mu}{\rho\lambda-\mu} (\omega_0^2 + \gamma_0^2) \gamma_0 \right] \int \frac{d^d k}{(2\pi)^d} \frac{\gamma_0 + D_0 k^2}{\omega_0^2 + (\gamma_0 + D_0 k^2)^2} \right. \\ \left. + \omega_0^2 \left[\omega_0^2 + \gamma_0^2 - \mu^2 - \frac{(\alpha-1)\mu}{\rho\lambda-\mu} (\omega_0^2 + \gamma_0^2) \right] \int \frac{(2\pi)^{-d} d^d k}{\omega_0^2 + (\gamma_0 + D_0 k^2)^2} \right. \\ \left. - \gamma_0 \left[\omega_0^2 + \gamma_0^2 - \mu(\gamma_0 - \mu) - \frac{(\alpha-1)\mu}{\rho\lambda-\mu} (\omega_0^2 + \gamma_0^2) \right] \int \frac{(2\pi)^{-d} d^d k}{\gamma_0 + D_0 k^2} \right). \quad (\text{A.6})$$

In the large prey carrying capacity limit $\rho \rightarrow \infty$ with $\gamma_0 \rightarrow 0$, these expression coincide and reduce to eq. (37).

Appendix B. Wavevector integrals

The required integrals are of the following form, and readily evaluated (where convergent in the ultraviolet) by means of Euler's Gamma function:

$$\int \frac{d^d k}{(2\pi)^d} \frac{k^{2\sigma}}{(\tau + k^2)^s} = \frac{1}{2^{d-1} \pi^{d/2} \Gamma(d/2)} \int_0^\infty \frac{k^{d-1+2\sigma}}{(\tau + k^2)^s} dk \\ = \frac{\Gamma(\sigma + d/2) \Gamma(s - \sigma - d/2)}{2^d \pi^{d/2} \Gamma(d/2) \Gamma(s)} \tau^{\sigma-s+d/2}. \quad (\text{B.1})$$

This immediately yields the basic integrals

$$\int \frac{d^d k}{(2\pi)^d} \frac{1}{\omega_0^2 + (\gamma_0 + D_0 k^2)^2} = -\frac{1}{\omega_0 D_0} \text{Im} \int \frac{d^d k}{(2\pi)^d} \frac{1}{k^2 + (\gamma_0 + i\omega_0)/D_0} \\ = -\frac{\Gamma(1-d/2)}{2^d \pi^{d/2}} \frac{\omega_0^{-2+d/2}}{D_0^{d/2}} \text{Im} \left(\frac{\gamma_0}{\omega_0} + i \right)^{-1+d/2}, \quad (\text{B.2})$$

$$\int \frac{d^d k}{(2\pi)^d} \frac{D_0 k^2}{\omega_0^2 + (\gamma_0 + D_0 k^2)^2} = -\frac{1}{\omega_0} \text{Im} \int \frac{d^d k}{(2\pi)^d} \frac{k^2}{k^2 + (\gamma_0 + i\omega_0)/D_0} \\ = \frac{\Gamma(1-d/2)}{2^d \pi^{d/2}} \frac{\omega_0^{-1+d/2}}{D_0^{d/2}} \text{Im} \left(\frac{\gamma_0}{\omega_0} + i \right)^{d/2}, \quad (\text{B.3})$$

$$\int \frac{d^d k}{(2\pi)^d} \frac{\gamma_0 + D_0 k^2}{\omega_0^2 + (\gamma_0 + D_0 k^2)^2} = \frac{1}{D_0} \text{Re} \int \frac{d^d k}{(2\pi)^d} \frac{1}{k^2 + (\gamma_0 + i\omega_0)/D_0} \\ = \frac{\Gamma(1-d/2)}{2^d \pi^{d/2}} \frac{\omega_0^{-1+d/2}}{D_0^{d/2}} \text{Re} \left(\frac{\gamma_0}{\omega_0} + i \right)^{-1+d/2}. \quad (\text{B.4})$$

This last result also follows from the sum of eqs. (B.2) and (B.3), if one observes that

$$\begin{pmatrix} \text{Re} \\ \text{Im} \end{pmatrix} \left(\frac{\gamma_0}{\omega_0} + i \right)^k = \frac{\gamma_0}{\omega_0} \begin{pmatrix} \text{Re} \\ \text{Im} \end{pmatrix} \left(\frac{\gamma_0}{\omega_0} + i \right)^{k-1} + \begin{pmatrix} -\text{Im} \\ \text{Re} \end{pmatrix} \left(\frac{\gamma_0}{\omega_0} + i \right)^{k-1}.$$

Next, decomposition into partial fractions gives

$$\begin{aligned} & \int \frac{d^d k}{(2\pi)^d} \frac{1}{\gamma_0 + D_0 k^2} \frac{1}{\omega_0^2 + (\gamma_0 + D_0 k^2)^2} \\ &= \frac{1}{\omega_0^2 D_0} \int \frac{d^d k}{(2\pi)^d} \left(\frac{1}{k^2 + \gamma_0/D_0} - \operatorname{Re} \frac{1}{k^2 + (\gamma_0 + i\omega_0)/D_0} \right) \\ &= \frac{\Gamma(1-d/2)}{2^d \pi^{d/2}} \frac{\omega_0^{-3+d/2}}{D_0^{d/2}} \left[\left(\frac{\gamma_0}{\omega_0} \right)^{-1+d/2} - \operatorname{Re} \left(\frac{\gamma_0}{\omega_0} + i \right)^{-1+d/2} \right], \quad (\text{B.5}) \end{aligned}$$

$$\begin{aligned} & \int \frac{d^d k}{(2\pi)^d} \frac{D_0 k^2}{(\gamma_0 + D_0 k^2)^2} \frac{1}{\omega_0^2 + (\gamma_0 + D_0 k^2)^2} \\ &= \frac{1}{\omega_0^2 D_0} \int \frac{d^d k}{(2\pi)^d} \left(\frac{k^2}{(k^2 + \gamma_0/D_0)^2} - \frac{k^2}{(k^2 + \gamma_0/D_0)^2 + \omega_0^2/D_0^2} \right) \\ &= \frac{\Gamma(1-d/2)}{2^d \pi^{d/2}} \frac{\omega_0^{-3+d/2}}{D_0^{d/2}} \left[\frac{d}{2} \left(\frac{\gamma_0}{\omega_0} \right)^{-1+d/2} - \operatorname{Im} \left(\frac{\gamma_0}{\omega_0} + i \right)^{d/2} \right]. \quad (\text{B.6}) \end{aligned}$$

Taking derivatives with respect to the parameters γ_0 and/or ω_0 one then obtains:

$$\begin{aligned} & \int \frac{d^d k}{(2\pi)^d} \frac{\gamma_0 + D_0 k^2}{[\omega_0^2 + (\gamma_0 + D_0 k^2)^2]^2} = -\frac{1}{2} \frac{\partial}{\partial \gamma_0} \int \frac{d^d k}{(2\pi)^d} \frac{1}{\omega_0^2 + (\gamma_0 + D_0 k^2)^2} \\ &= -\frac{\Gamma(2-d/2)}{2^{d+1} \pi^{d/2}} \frac{\omega_0^{-3+d/2}}{D_0^{d/2}} \operatorname{Im} \left(\frac{\gamma_0}{\omega_0} + i \right)^{-2+d/2}, \quad (\text{B.7}) \end{aligned}$$

$$\begin{aligned} & \int \frac{d^d k}{(2\pi)^d} \frac{D_0 k^2}{[\omega_0^2 + (\gamma_0 + D_0 k^2)^2]^2} = -\frac{1}{2\omega_0} \frac{\partial}{\partial \omega_0} \int \frac{d^d k}{(2\pi)^d} \frac{D_0 k^2}{\omega_0^2 + (\gamma_0 + D_0 k^2)^2} \\ &= \frac{\Gamma(1-d/2)}{2^{d+1} \pi^{d/2}} \frac{\omega_0^{-3+d/2}}{D_0^{d/2}} \left[\operatorname{Im} \left(\frac{\gamma_0}{\omega_0} + i \right)^{d/2} - \frac{d}{2} \operatorname{Re} \left(\frac{\gamma_0}{\omega_0} + i \right)^{-1+d/2} \right], \quad (\text{B.8}) \end{aligned}$$

$$\begin{aligned} & \int \frac{d^d k}{(2\pi)^d} \frac{1}{[\omega_0^2 + (\gamma_0 + D_0 k^2)^2]^2} = -\frac{\Gamma(1-d/2)}{2^{d+1} \pi^{d/2}} \frac{\omega_0^{-4+d/2}}{D_0^{d/2}} \operatorname{Im} \left(\frac{\gamma_0}{\omega_0} + i \right)^{-1+d/2} \\ &\quad - \frac{\Gamma(2-d/2)}{2^{d+1} \pi^{d/2}} \frac{\omega_0^{-4+d/2}}{D_0^{d/2}} \operatorname{Re} \left(\frac{\gamma_0}{\omega_0} + i \right)^{-2+d/2}, \quad (\text{B.9}) \end{aligned}$$

$$\begin{aligned} & \int \frac{d^d k}{(2\pi)^d} \frac{D_0 k^2 (\gamma_0 + D_0 k^2)}{[\omega_0^2 + (\gamma_0 + D_0 k^2)^2]^3} = -\frac{d\Gamma(1-d/2)}{2^{d+4} \pi^{d/2}} \frac{\omega_0^{-4+d/2}}{D_0^{d/2}} \operatorname{Im} \left(\frac{\gamma_0}{\omega_0} + i \right)^{-1+d/2} \\ &\quad - \frac{d\Gamma(2-d/2)}{2^{d+4} \pi^{d/2}} \frac{\omega_0^{-4+d/2}}{D_0^{d/2}} \operatorname{Re} \left(\frac{\gamma_0}{\omega_0} + i \right)^{-2+d/2}, \quad (\text{B.10}) \end{aligned}$$

$$\begin{aligned} & \int \frac{d^d k}{(2\pi)^d} \frac{1}{\gamma_0 + D_0 k^2} \frac{1}{[\omega_0^2 + (\gamma_0 + D_0 k^2)^2]^2} \\ &= \frac{\Gamma(1-d/2)}{2^d \pi^{d/2}} \frac{\omega_0^{-5+d/2}}{D_0^{d/2}} \left[\left(\frac{\gamma_0}{\omega_0} \right)^{-1+d/2} - \operatorname{Re} \left(\frac{\gamma_0}{\omega_0} + i \right)^{-1+d/2} \right] \\ &\quad + \frac{\Gamma(2-d/2)}{2^{d+1} \pi^{d/2}} \frac{\omega_0^{-5+d/2}}{D_0^{d/2}} \operatorname{Im} \left(\frac{\gamma_0}{\omega_0} + i \right)^{-2+d/2}, \quad (\text{B.11}) \end{aligned}$$

$$\int \frac{d^d k}{(2\pi)^d} \frac{\gamma_0 + D_0 k^2}{[\omega_0^2 + (\gamma_0 + D_0 k^2)^2]^3} = -\frac{\Gamma(2-d/2)}{2^{d+3} \pi^{d/2}} \frac{\omega_0^{-5+d/2}}{D_0^{d/2}} \operatorname{Im}\left(\frac{\gamma_0}{\omega_0} + i\right)^{-2+d/2} - \frac{\Gamma(3-d/2)}{2^{d+3} \pi^{d/2}} \frac{\omega_0^{-5+d/2}}{D_0^{d/2}} \operatorname{Re}\left(\frac{\gamma_0}{\omega_0} + i\right)^{-3+d/2}, \quad (\text{B.12})$$

$$\begin{aligned} \int \frac{d^d k}{(2\pi)^d} \frac{D_0 k^2}{[\omega_0^2 + (\gamma_0 + D_0 k^2)^2]^3} &= \frac{3\Gamma(1-d/2)}{2^{d+3} \pi^{d/2}} \frac{\omega_0^{-5+d/2}}{D_0^{d/2}} \left[\operatorname{Im}\left(\frac{\gamma_0}{\omega_0} + i\right)^{d/2} - \frac{d}{2} \operatorname{Re}\left(\frac{\gamma_0}{\omega_0} + i\right)^{-1+d/2} \right] \\ &\quad + \frac{d\Gamma(2-d/2)}{2^{d+4} \pi^{d/2}} \frac{\omega_0^{-5+d/2}}{D_0^{d/2}} \operatorname{Im}\left(\frac{\gamma_0}{\omega_0} + i\right)^{-2+d/2}, \quad (\text{B.13}) \end{aligned}$$

$$\begin{aligned} \int \frac{d^d k}{(2\pi)^d} \frac{1}{[\omega_0^2 + (\gamma_0 + D_0 k^2)^2]^3} &= -\frac{3\Gamma(1-d/2)}{2^{d+3} \pi^{d/2}} \frac{\omega_0^{-6+d/2}}{D_0^{d/2}} \operatorname{Im}\left(\frac{\gamma_0}{\omega_0} + i\right)^{-1+d/2} \\ &\quad - \frac{3\Gamma(2-d/2)}{2^{d+3} \pi^{d/2}} \frac{\omega_0^{-6+d/2}}{D_0^{d/2}} \operatorname{Re}\left(\frac{\gamma_0}{\omega_0} + i\right)^{-2+d/2} \\ &\quad + \frac{\Gamma(3-d/2)}{2^{d+3} \pi^{d/2}} \frac{\omega_0^{-6+d/2}}{D_0^{d/2}} \operatorname{Im}\left(\frac{\gamma_0}{\omega_0} + i\right)^{-3+d/2}, \quad (\text{B.14}) \end{aligned}$$

$$\begin{aligned} \int \frac{d^d k}{(2\pi)^d} \frac{D_0 k^2 (\gamma_0 + D_0 k^2)}{[\omega_0^2 + (\gamma_0 + D_0 k^2)^2]^4} &= -\frac{d\Gamma(1-d/2)}{2^{d+5} \pi^{d/2}} \frac{\omega_0^{-6+d/2}}{D_0^{d/2}} \operatorname{Im}\left(\frac{\gamma_0}{\omega_0} + i\right)^{-1+d/2} \\ &\quad - \frac{d\Gamma(2-d/2)}{2^{d+5} \pi^{d/2}} \frac{\omega_0^{-6+d/2}}{D_0^{d/2}} \operatorname{Re}\left(\frac{\gamma_0}{\omega_0} + i\right)^{-2+d/2} \\ &\quad + \frac{d\Gamma(3-d/2)}{3 \cdot 2^{d+5} \pi^{d/2}} \frac{\omega_0^{-6+d/2}}{D_0^{d/2}} \operatorname{Im}\left(\frac{\gamma_0}{\omega_0} + i\right)^{-3+d/2}, \quad (\text{B.15}) \end{aligned}$$

$$\begin{aligned} \int \frac{d^d k}{(2\pi)^d} \frac{D_0 k^2}{[\omega_0^2 + (\gamma_0 + D_0 k^2)^2]^4} &= \frac{5\Gamma(1-d/2)}{2^{d+4} \pi^{d/2}} \frac{\omega_0^{-7+d/2}}{D_0^{d/2}} \left[\operatorname{Im}\left(\frac{\gamma_0}{\omega_0} + i\right)^{d/2} - \frac{d}{2} \operatorname{Re}\left(\frac{\gamma_0}{\omega_0} + i\right)^{-1+d/2} \right] \\ &\quad + \frac{d\Gamma(2-d/2)}{2^{d+4} \pi^{d/2}} \frac{\omega_0^{-7+d/2}}{D_0^{d/2}} \operatorname{Im}\left(\frac{\gamma_0}{\omega_0} + i\right)^{-2+d/2} \\ &\quad + \frac{d\Gamma(3-d/2)}{3 \cdot 2^{d+5} \pi^{d/2}} \frac{\omega_0^{-7+d/2}}{D_0^{d/2}} \operatorname{Re}\left(\frac{\gamma_0}{\omega_0} + i\right)^{-3+d/2}. \quad (\text{B.16}) \end{aligned}$$

For explicit evaluation at $d = 2$, the Gamma function $\Gamma(1 - d/2)$ diverges, but its poles in the expressions for the renormalized oscillation parameters are all cancelled, as can be checked by setting $d = 2 - \varepsilon$, and carefully taking the limit $\varepsilon \rightarrow 0$. Indeed, the singularities in two dimensions are eliminated by the counter-terms A_c and B_c . At $d = 4$, ultraviolet divergences appear, which must be regularized by a cut-off Λ in momentum space that originates from the underlying lattice; e.g., $\Lambda = 2\pi/a_0$ in a hypercubic lattice with lattice constant a_0 . In the above integral listing, these ultraviolet singularities

emerge as poles in $\epsilon = 4 - d$; the precise correspondence with the cut-off regularization is $\Gamma(1 + \epsilon/2)/\epsilon(1 - \epsilon/2) \rightarrow \frac{1}{4} \ln(1 + \Lambda^4 D_0^2/\omega_0^2)$.

References

- [1] May R M 1973 *Stability and complexity in model ecosystems*, (Princeton: Princeton University Press)
- [2] Maynard Smith J 1974 *Models in ecology* (Cambridge: Cambridge University Press)
- [3] Hofbauer J and Sigmund K 1998 *Evolutionary games and population dynamics* (Cambridge: Cambridge University Press)
- [4] Murray J D 2002 *Mathematical biology*, Vols. I and II (New York: Springer, 3rd ed.)
- [5] Durrett R 1999 *SIAM Review* **41** 677
- [6] Lotka A J 1920 *Proc. Natl. Acad. Sci. U.S.A.* **6** 410; *J. Amer. Chem. Soc.* **42** 1595
- [7] Volterra V 1926 *Mem. Accad. Lincei* **2** 31
- [8] Matsuda H, Ogita N, Sasaki A and Satō K 1992 *Prog. Theor. Phys.* **88** 1035
- [9] Satulovsky J E and Tomé T 1994 *Phys. Rev. E* **49** 5073
- [10] Boccara N, Roblin O and Roger M 1994 *Phys. Rev. E* **50** 4531
- [11] Mobilia M, Georgiev I T and Täuber UC 2007 *J. Stat. Phys.* **128** 447
- [12] Provata A, Nicolis G and Baras F 1999 *J. Chem. Phys.* **110** 8361
- [13] Rozenfeld A F and Albano E V 1999 *Physica A* **266** 322
- [14] Lipowski A 1999 *Phys. Rev. E* **60** 5179
- [15] Lipowski A and Lipowska D 2000 *Physica A* **276** 456
- [16] Monetti R, Rozenfeld A F and Albano E V 2000 *Physica A* **283** 52
- [17] Droz M and Pekalski A 2001 *Phys. Rev. E* **63** 051909
- [18] Antal T and Droz M 2001 *Phys. Rev. E* **63** 056119
- [19] Kowalik M, Lipowski A and Ferreira A L 2002 *Phys. Rev. E* **66** 066107
- [20] McKane A J and Newman T J 2005 *Phys. Rev. Lett.* **94** 218102
- [21] Parker M and Kamenev A 2009 *Phys. Rev. E* **80** 021129
- [22] Dobrinevski A and Frey E 2012 *Phys. Rev. E* **85** 051903
- [23] Dunbar S R 1983 *J. Math. Biol.* **17** 11
- [24] Sherratt J, Eagen B T and Lewis M A 1997 *Phil. Trans. R. Soc. Lond. B* **352** 21
- [25] de Aguiar M A M, Rauch A M and Bar-Yam Y 2004 *J. Stat. Phys.* **114** 1417
- [26] Movies of Monte Carlo simulation runs with various parameter settings can be viewed at:
<http://www.phys.vt.edu/~tauber/PredatorPrey/movies/>
- [27] Washenberger M J, Mobilia M and Täuber UC 2007 *J. Phys. Condens. Matter* **19** 065139
- [28] Mobilia M, Georgiev I T and Täuber U C 2006 *Phys. Rev. E* **73**, 040903(R)
- [29] Dobramysl U and Täuber U C 2008 *Phys. Rev. Lett.* **101**, 258102
- [30] Doi M 1976 *J. Phys. A: Math. Gen.* **9** 1465
- [31] Grassberger P and Scheunert P 1980 *Fortschr. Phys.* **28** 547
- [32] Peliti L 1985 *J. Phys. (France)* **46** 1469; 1479
- [33] Lee B P 1994 *J. Phys. A: Math. Gen.* **27** 2633
- [34] Mattis D C and Glasser M L 1998 *Rev. Mod. Phys.* **70** 979
- [35] Täuber U C, Howard M and Vollmayr-Lee B P 2005 *J. Phys. A: Math. Gen.* **38** R79
- [36] van Wijland F 2001 *Phys. Rev. E* **63** 022101
- [37] A concise preliminary summary of some of the results can be found in:
Täuber U C 2011 *J. Phys.: Conf. Ser.* **319** 012019
- [38] Obukhov S P 1980 *Physica A* **101** 145
- [39] Cardy J L and Sugar R L 1980 *J. Phys. A: Math. Gen.* **13** L423
- [40] Janssen H K 1981 *Z. Phys. B* **42** 151
- [41] Janssen H K and Täuber U C 2005 *Ann. Phys.* **315** 147
- [42] Grassberger P 1982 *Z. Phys. B* **47** 365

- [43] Hinrichsen H 2000 *Adv. Phys.* **49** 815
- [44] Janssen H K 2001 *J. Stat. Phys.* **103** 801
- [45] Ódor G 2004 *Rev. Mod. Phys.* **76** 663
- [46] Butler T and Reynolds D 2009 *Phys. Rev. E* **79** 032901
- [47] Täuber U C 2007 *Field theory approaches to nonequilibrium dynamics*, in: Henkel M, Pleimling M and Sanctuary R (eds) *Ageing and the glass transition*, Lecture Notes in Physics **716** (Berlin: Springer) 295
- [48] Täuber U C 2009 *Field-theoretic methods*, in: Meyers R A (ed) *Encyclopedia of complexity and system science* (New York: Springer) 3360
- [49] Negele J W and Orland H 1988 *Quantum many-particle systems* (Redwood City: Addison-Wesley)
- [50] Janssen H K 1976 *Z. Phys. B* **23** 377
- [51] De Dominicis C 1976 *J. Phys. (France) Colloq.* **37** C2247
- [52] Brézin E and Wallace D J 1973 *Phys. Rev. B* **7** 1967
- [53] Lawrie I D 1981 *J. Phys. A: Math. Gen.* **14** 2489
- [54] Täuber U C and Schwabl F 1992 *Phys. Rev. B* **46** 3337
- [55] He Q, Mobilia M and Täuber U C 2010 *Phys. Rev. E* **82** 051909
- [56] He Q, Mobilia M and Täuber U C 2011 *Eur. Phys. J. B* **82** 97
- [57] He Q, Zia R K P and Täuber U C 2012 *Eur. Phys. J. B* **85** 141